Universidad Carlos III de Madrid

Bachelor's Degree in Biomedical Engineering

Bachelor Thesis

4D IMAGING OF HEART VASO-ARCHITECTURE AFTER MYOCARDIAL INFARCTION

Author

Alicia Arévalo García

Tutor

Manuel Desco Menéndez

Co-director

María Victoria Gómez Gaviro

September 2017

This page was intentionally left blank

INDEX

ABSTRACT

Cardiovascular diseases remain the number one cause of death globally. There is an ongoing desire to study the distribution and structural changes of the vaso-architecture in the diseased heart in cardiovascular research groups all over the world.

The ability to acquire high resolution 3D-images of the heart vasculature enables to study heart diseases more in detail and eventually obtain interesting new findings and new treatments. In this work, we introduce a pipeline for high resolution 3D-imaging of the changes in mouse heart vasculature after a myocardial infarction is produced with Single Plane Illumination Microscopy (SPIM).

To achieve high resolution 3D-images, protocols for optical tissue clearing (CUBIC tissue clearing technique) were combined with vasculature labelling methods (IHC and intravenous perfused lectin), enabling the visualization for the very first time of the whole heart vasculature.

We here also describe the methods used for image pre-processing of the acquired data, mainly for correction of SPIM-image artifacts and for segmentation of the structures of interest.

Finally, the analysis of the changes in vasculature between healthy hearts with the different stages of chronic myocardial infarction (7, 14 and 28 days post-infarction) will provide us a tool to know how this disease affects not only to infarcted region but to the whole heart volume.

1. INTRODUCTION

1.1. MOTIVATION AND MEDICAL BACKGROUND

Coronary artery disease (CAD), also known as ischemic heart disease (IHD), is a group of diseases that includes stable angina, unstable angina, myocardial infarction (MI) and sudden cardiac death. They are the world's biggest killers, accounting for 9 million deaths in Europe in 2015. Furthermore, CAD have remained the leading causes of death globally in the last 15 years [1].

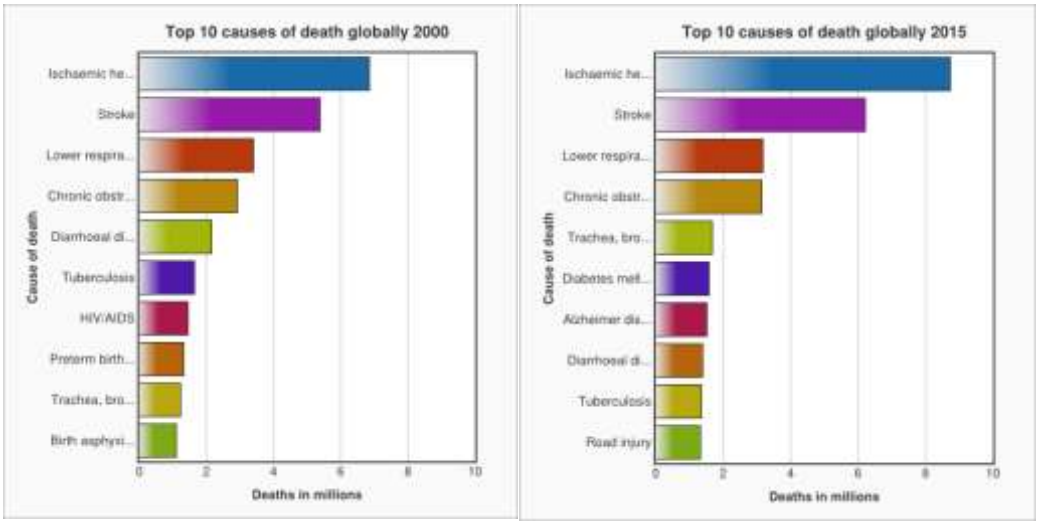

Figure 1. Top 10 causes of death globally in 2010 and 2015 in Europe, from [1].

The animal model of myocardial infarction (MI) plays an important role in the prevention, diagnosis, and therapy of human MI. The study of the behavior of heart vaso-architecture after MI is produced and its evaluation along time in a 4-dimension (4D) analysis will provide an insight into this disease. The 4D images to be analyzed in this work were acquired with light sheet fluorescence microscopy (LSFM) technology which suppose an innovative and advantageous approach to whole volume analysis of damaged areas that previous microscopy techniques couldn't allow.

1.2. HEART – VASCULATURE TREE

The heart is defined as a hollow organ which pumps blood throughput the body and that, along with the blood and the blood vessels, constitute the cardiovascular system.

The heart has four chambers. The two superior receiving chambers are the atria (entry chambers), and the two inferior pumping chambers are the ventricles (little bellies). The paired atria receive blood from blood vessels returning blood to the heart, called veins, while the ventricles eject the blood from the heart into blood vessels called arteries. On the anterior surface of each atrium is a wrinkled pouchlike structure called auricle. Each auricle slightly increases the capacity of an atrium so that it can hold a greater volume of blood. Also on the surface of the heart are a series of grooves, called sulci, which contain coronary blood vessels and a variable amount of fat. Each sulcus marks the external boundary between two chambers of the heart (Fig. 2.A).

The right atrium forms the right border of the heart and receives blood from three veins: the superior vena cava, inferior vena cava, and coronary sinus. The anterior and posterior walls of the right atrium are very different. Blood passes from the right atrium into the right ventricle through a valve that is called the tricuspid valve.

The right ventricle forms most of the anterior surface of the heart. The inside of the right ventricle contains a series of ridges formed by raised bundles of cardiac muscle fibers called trabeculae carneae. Some of the trabeculae carneae convey part of the conduction system of the heart. Blood passes from the right ventricle through the pulmonary valve into a large artery called the pulmonary trunk, which carries blood to the lungs.

The left atrium forms most of the base of the heart. It receives blood from the lungs through four pulmonary veins. Like the right atrium, the inside of the left atrium has a smooth posterior wall.

The left ventricle is the thickest chamber of the heart and forms the apex of the heart. Like the right ventricle, the left ventricle contains trabeculae carneae. Blood passes from the left ventricle through the aortic valve into the ascending aorta. Some of the blood in the aorta flows into the coronary arteries, which branch from the ascending aorta and carry blood to the heart wall. The remainder of the blood passes into the arch of the aorta and

descending aorta. Branches of the arch of the aorta and descending aorta carry blood throughout the body.

Although it is considered as a whole muscle, the heart wall consists of three different layers: the epicardium, the myocardium and the endocardium (see Fig. 2.B).

The epicardium is the external layer. It is composed itself of two tissue layers. The outermost is called the visceral layer of the serous pericardium, the membrane that protects and surround the heart. This thin, transparent outer layer of the heart wall is composed of mesothelium. Beneath the mesothelium is a variable layer of delicate fibroelastic tissue and adipose tissue. The adipose tissue predominates and becomes thickest over the ventricular surfaces, where it houses the major coronary and cardiac vessels of the heart. The epicardium imparts a smooth, slippery texture to the outermost surface of the heart. The epicardium contains blood vessels, lymphatics, and vessels that supply the myocardium.

The middle layer, the myocardium, is responsible for the pumping action of the heart and is composed of cardiac muscle tissue. It makes up approximately 95% of the heart wall. The muscle fibers (cells), like those of striated skeletal muscle tissue, are wrapped and bundled with connective tissue sheaths composed of endomysium and perimysium. The cardiac muscle fibers are organized in bundles that swirl diagonally around the heart and generate the strong pumping actions of the heart. Although it is striated like skeletal muscle, recall that cardiac muscle is involuntary like smooth muscle.

The innermost endocardium is a thin layer of endothelium overlying a thin layer of connective tissue. It provides a smooth lining for the chambers of the heart and covers the valves of the heart. The smooth endothelial lining minimizes the surface friction as blood passes through the heart. The endocardium is continuous with the endothelial lining of the large blood vessels attached to the heart.

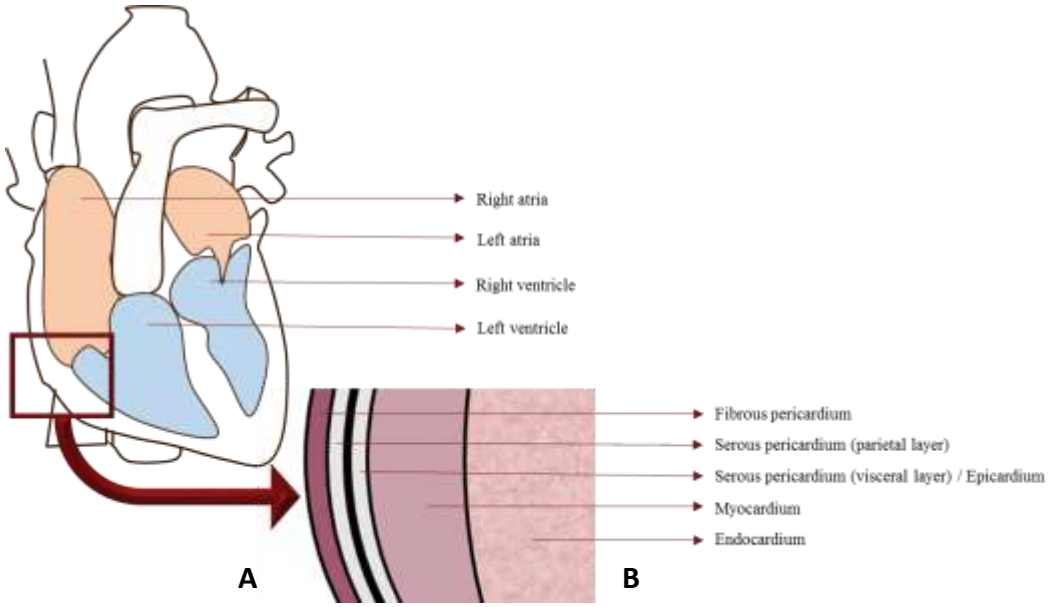

Figure 2. A: sketch of heart chambers. **B**: sketch of wall structure.

Nutrients are not able to diffuse quickly enough from blood in the chambers of the heart to supply all the layers of cells that make up the heart wall. For this reason, the myocardium has its own network of blood vessels, the coronary circulation. The coronary arteries branch from the ascending aorta and encircle the heart like a crown encircles the head. While the heart is contracting, little blood flows in the coronary arteries because they are squeezed shut. When the heart relaxes, however, the high pressure of blood in the aorta propels blood through the coronary arteries, into capillaries, and then into coronary veins.

Two coronary arteries, the right and left coronary arteries, branch from the ascending aorta and supply oxygenated blood to the myocardium (Fig. 3).

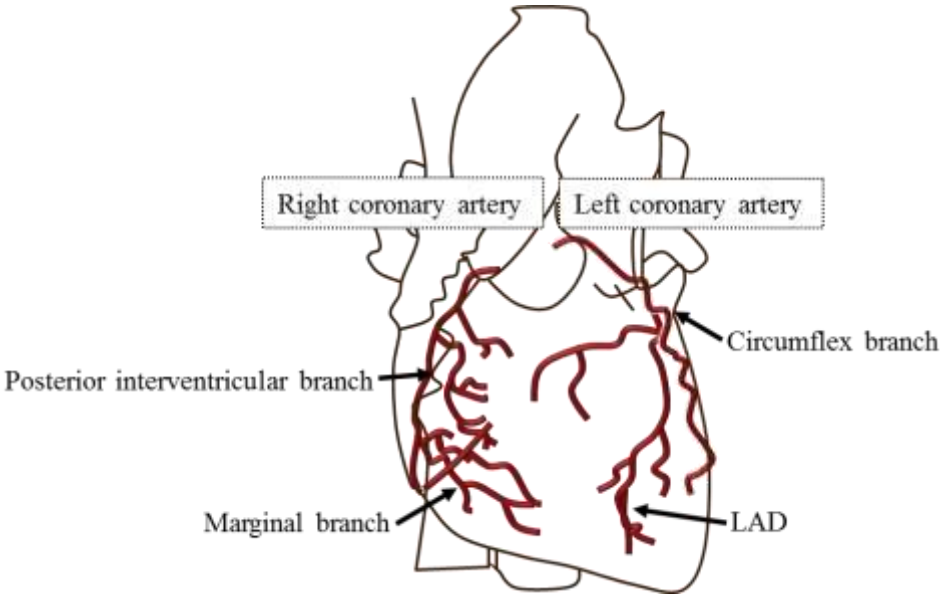

Figure 3. Right and left coronary arteries sketch.

The left coronary artery passes inferior to the left auricle and divides into the anterior interventricular and circumflex branches. The anterior interventricular branch or left anterior descending (LAD) artery supplies oxygenated blood to the walls of both ventricles. The circumflex branch distributes oxygenated blood to the walls of the left ventricle and left atrium.

The right coronary artery supplies small branches (atrial branches) to the right atrium. It continues inferior to the right auricle and ultimately divides into the posterior interventricular and marginal branches. The posterior interventricular branch supplies the walls of the two ventricles with oxygenated blood. The marginal branch transports oxygenated blood to the myocardium of the right ventricle.

Most parts of the body receive blood from branches of more than one artery, and where two or more arteries supply the same region, they usually connect. These connections, called anastomoses, provide alternate routes, called collateral circulation, for blood to reach a particular organ or tissue.

The myocardium contains many anastomoses that connect branches of a given coronary artery or extend between branches of different coronary arteries. They provide detours for

arterial blood if a main route becomes obstructed. Thus, heart muscle may receive sufficient oxygen even if one of its coronary arteries is partially blocked [2].

Coronary artery disease (CAD), also known as ischemic heart disease (IHD), is a group of diseases that includes stable angina, unstable angina, myocardial infarction (MI) and sudden cardiac death.

Myocardial infarction, commonly called a heart attack, is the most likely outcome of CAD. It is produced by a complete obstruction to blood flow in a coronary artery. Infarction means the death of an area of tissue because of interrupted blood supply. As a consequence of the death of heart tissue distal to the obstruction and its replacement by non-contractile scar tissue, the heart muscle loses some of its strength or even die.

1.3. FLUORESCENCE MICROSCOPY - SPIM

The principle of the basic optical microscopy is the use of a source of visible light and an arrangement of lenses achieving high magnification imaging of small or thin samples. Although it is not clear who was the inventor of the microscope, its invention is documented to have taken place in the late 15th to early 16th century. Zaccharias Janssen and his competitor Hans Lippershey are both suspected to have constructed a compound microscope in 1590, but until 1609 there wasn't a device that received the name "microscope". This first microscope was the one built by Galileo Galilei.

Optical microscopy has played a fundamental role in cell and molecular biology since 17th century when Antoni van Leeuwenjoek used a home-made microscope to describe single-cell organisms such as bacteria or microorganisms [3]. Even though light microscopes have been available for over four centuries, a major breakthrough in microscopy was the development of fluorescence microscopy. Its promising potential emerged with the discovery of fluorescence by the British Sir George G. Stokes in 1852 but it was not until the 1930s that fluorophores started to be used in biomedical scientific investigations [4].

Fluorescence phenomena are defined as the absorption and subsequent emission of light by a sample. Fluorophores can be broadly divided into two main classes—intrinsic and extrinsic. Intrinsic fluorophores are those that occur naturally while extrinsic fluorophores

are added to the sample to provide fluorescence when none exists, or to change the spectral properties of the sample [5]. Thus, the sample under study may naturally contain the fluorophore, be genetically modified to express it e.g. in form of Green Fluorescent Protein (GFP) and its variations, or it can be chemically manipulated by labeling specific cells or proteins through a process called "Immunohistochemistry" (IHC). In fluorescence microscopy the biological sample containing a fluorophore is illuminated through the objective lens with a narrow set of wavelengths of light. The light interacts with the fluorophore, which emits back radiation of a longer wavelength that is caught on the detector. Between the photon absorption and its emission there is a very short time delay, usually less than a microsecond, causing it to be a nearly simultaneous event.

Fluorescence microscopy is based on the concept of fluorescence discovered by Sir George G. Stokes in 1852 [6]. Typically a Jablonski diagram is used to illustrate the physics of fluorescence.

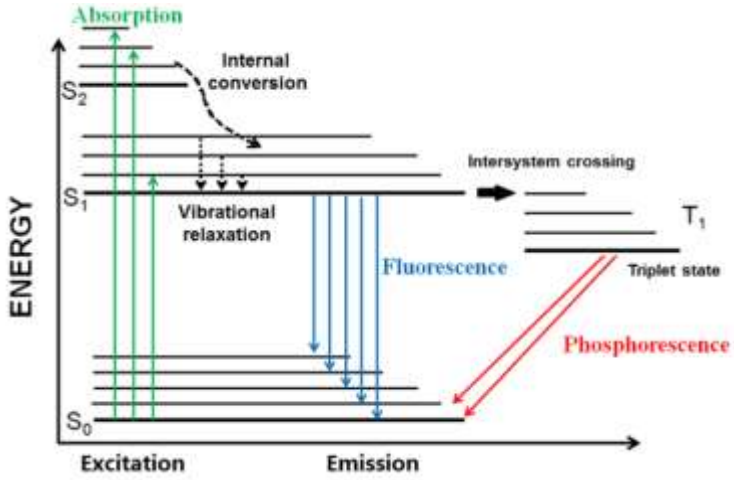

Figure 4. Simplified Jablonski diagram. A fluorescent molecule is able to absorb light energy (through the process called excitation) and emits rapidly fluorescence (through the process of emission). From the excited state S1, other pathways for relaxation exist. Radiationless decay happens through internal conversion or intersystem crossing to a triplet state. The intersystem crossing may subsequently relax through a process called phosphorescence. Fluorescence emission occurs from the vibrational minimum of S1 to S0. The return to the S0 state can also occur through interaction with a second molecule through fluorescence quenching (not shown in the diagram). Image from [7].

Another revolutionary innovation in microscopy was the development of the digital microscope that incorporates a "charge-coupled device"-camera (CCD-camera) onto which

the optical image is projected, allowing its digital visualization on a monitor, image data acquisition and further image processing. However, the most common fluorescence microscope configuration is known as “epi-fluorescence” microscopy. In epi-fluorescence microscopy the sample under study needs to be processed through histological sectioning in very thin slices (from 5 to 50μm) due to the limitations of the working distance of the imaging objectives and the transparency of the sample, in order to yield high-resolution images. Main drawbacks of this technique are that the cutting of the sample often produces distortion of the sample and imaging artifacts. Another important limitation is the low tissue penetration of light and the out of focus fluorescence, since the standard fluorescence microscope captures emitted light from all the illuminated planes in the sample and not only from the actual plane in focus. These constraints have been overcome with the development of optical sectioning microscopy such as Confocal and Light sheet fluorescence microscopy (LSFM). The objective of these types of microscopy is avoiding the physical section of the samples. The sectioning is achieved with the laser light. LSFM or Single Plane Illumination Microscopy (SPIM) allows acquiring high-resolution images through a large specimen at different axial depths. Good optical sectioning allows a straightforward 3D-reconstruction of a 2D-image stack into a volumetric data set.

SINGLE PLANE ILLUMINATION MICROSCOPY (SPIM)

SPIM approaches the optical sectioning technology with a different configuration. The laser illuminates the sample in the form of a light sheet formed by a cylindrical lens collocated in the path of the laser light. This leads to fluorescence excitation exclusively in a very thin sheet-like volume. So, only the light emission specific to that particular slice is detected. Figure 5 shows a schematized SPIM set-up.

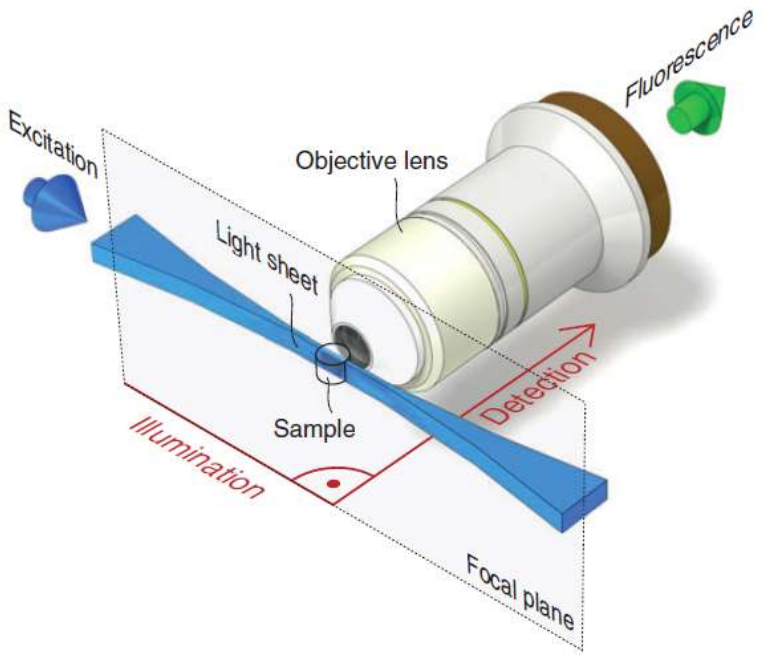

Figure 5. The width of the beam is broader at the ends and narrower towards the center.

In SPIM the illumination and the detection paths are orthogonal to each other. The sample is placed in the focal plane at the intersection of the two perpendicular axes. The sample is moved stepwise along the z-axial direction to acquire parallel planar images through the whole sample volume. The specimen is moved using a step motor with micro-metric precision. The static sheet of light used in SPIM is created using a cylindrical lens which is collocated in the light path of the laser. The excitation laser light is directed through a set of mirrors until reaching a cylindrical lens, which forms the light sheet. The laser light is focused planar. The thickness of the light sheet limits the achievable z-axial resolution of the data set. Although it ideally should be close to negligible, it usually presents a thickness of a few micrometers. The beam has a Gaussian shape as it can be seen in Fig. 5. The width of the beam is broader at the ends and narrower towards the center.

By placing the sample in the narrowest part of the light sheet, the sample will be illuminated with the most uniform part of it. Technical limitations are outpaced by the following diverse improvements that the SPIM technology offers in the domain of wide field fluorescence microscopy. The microscope configuration is accessible and versatile and

modern high sensitivity CCD and Complementary Metal Oxide Silicon (CMOS) cameras allow fast acquisition of high quality images [3]. One important benefit of SPIM is the reduced photobleaching and phototoxicity in the sample since excitation radiation is received only by the sheet-like volume that is illuminated only for a short time. In comparison with the other fluorescence microscopy modalities in which the whole sample is excited during the entire time span of the scanning, the reduction in photobleaching can reach up to several orders of magnitude. Furthermore, this powerful instrument allows imaging with cellular resolution. The lateral resolution of the system is fully determined by the detection optics and the wavelength of the emitted light, according to the Rayleigh equation:

$$r = 0.61 \frac{\lambda}{NA}$$

Where r is the minimum distance between two distinguishable points, i.e. the minimum distance for the two points to be perceived as separate. ¸ is the excitation light wave length in nm and NA (dimensionless) is the numerical aperture of the objective lens.

The numerical aperture is defined as the total range of angles over which the objective lens can gather light. The axial resolution is limited by the laser sheet thickness and the precision of the step motor that moves the sample. The motorized stages used in the set-up of the SPIM microscope move with micro-metric precision, allowing an axial resolution as low as a few micrometers. The acquisition of the data set in form of a stack of high quality 2D-images allows the straightforward reconstruction of a 3D-volume. Whole organisms and multicellular samples can quickly be 3D-imaged. The variety of excitation lasers of different wavelengths together with the availability of different markers allows labeling the same specimen with more than one fluorophore. Multiple channels can be acquired sequentially by simply changing the excitation laser wavelength and the corresponding emission filter. SPIM makes possible imaging of relatively large biological tissue samples, organs of small animals or whole organisms such as embryos. The main limitation is the barrier of light penetration through the tissue. A ballistic propagation of the excitation laser sheet through the sample is desired. At the same time, the emitted fluorescence light is expected to

escape the sample and reach the detection objective. Tissues present optical absorption and scattering properties that hinder the uniform light propagation through the tissue [8]. In order to compensate for this limitation and minimize the absorption and scattering that light suffers when interacting with tissues, specimens need to be either sufficiently thin or present a high degree of transparency.

1.4. OPTICAL TISSUE CLEARING

The imaging depth in optical microscopy is limited by tissue opacity and light penetration. In an attempt to overcome the limitation of tissue light scattering and absorption diverse approaches have been developed over the past decade. Optical clearing techniques aim for rendering biological specimen transparent using physical procedures and chemical agents. Since light scattering occurs at the boundary between materials with different refractive indices, most of the modern clearing methods involve treating the sample with organic solvents in order to homogenize the refractive indices inside the sample. Lipids are molecules that constitute a major source of light scattering. Therefore almost all techniques involve the removal of lipids. Fig. 6 shows a sketch of the excitation laser light penetration into uncleared and cleared tissue.

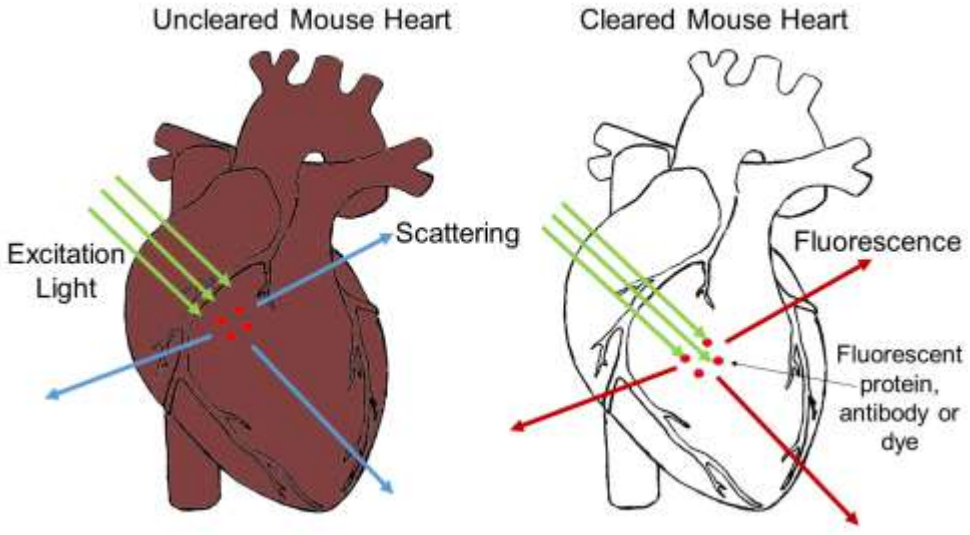

Figure 6. Light scattering properties of biological tissues do not let the light of the excitation laser penetrate to excite the fluorophores inside the sample. After clearing of the tissue

the excitation laser light reaches to the fluorophores and imaging can be achieved. Figure adapted from [9].

Many biocompatible chemical agents have been tested in order to maximize the optical clearing efficacy. Methods such as Scale [10], BABB [11], SeeDB [12], iDISCO [13], CLARITY [14] and CUBIC [15] investigated the numerous options of mixing different alcohols, sugars, organic acids and other organic solvents. All optical clearing techniques aim to achieve high transparency of relatively large samples while preserving the functional and anatomical information intact. Although the samples should not suffer physical deformation, tissue swelling is a common phenomenon in many of the mentioned clearing methods.

But the most important property is to preserve tissue organization at cellular and systemic level. Chemical-based mixtures used in clearing agents tend to cause quenching of transgenic fluorescent proteins or limit the life span of immuno-labeled fluorophores. Recently published methods such as CLARITY [14] and CUBIC [15] claim to have achieved a high degree of transparency while preserving the fluorescence signal and being compatible with IHC. A limitation of many clearing techniques is the long incubation period that is required, ranging from several weeks (CLARITY) to several months (Scale) to make organs of adult mice transparent. Some of them are logistically laborious to be replicated in the laboratory. E.g. in the case of the CLARITY method that actively removes the lipids by exposing the sample to electrophoresis, a specialized expensive electrophoresis device is required for this task. The CUBIC (Clear, Unobstructed Brain Imaging Cocktails) clearing method emerged recently as a relatively fast, replicable and inexpensive procedure that employs only two reagents to achieve highly transparent samples as described in mice brain and other murine organs. Passive immersion of the samples in urea, sucrose, detergents, alcohols and water is enough to remove lipids and homogenize the RIs in the sample.

Its simplicity and compatibility with IHC and SPIM makes it the method of choice in this work.

IMMUNOHISTOCHEMISTRY

Immunohistochemistry refers to the process of detecting antigens, for example proteins, in cells of a tissue section by taking advantage of the principle of antibodies binding to specific antigens. IHC-labeling is used to understand the distribution and localization of biomarkers and differently expressed proteins in different parts of a biological tissue. IHC on histological whole heart organs was performed for SPIM image acquisition.

A primary antibody (Ab) that binds specifically to an antigen is used to target a specific cell type. Visualization of the distribution of the primary antibody is achieved by a secondary antibody labeled with a fluorophore molecule that binds specifically to the primary antibody. The secondary antibody must be chosen depending on the host species in which the primary antibody was raised. See Fig. 7.

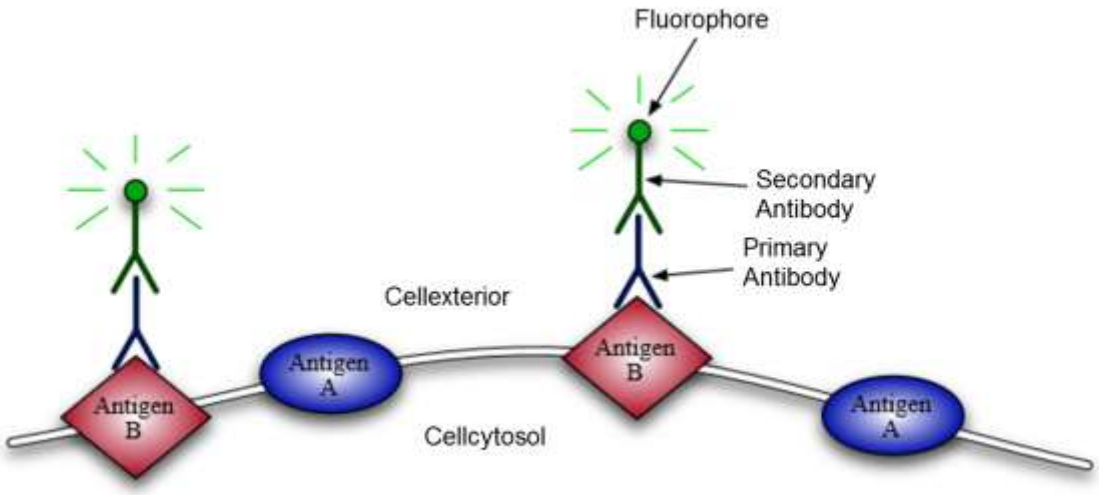

Figure 7. Principle of IHC: The primary antibody binds specifically to the antigen named B. The secondary antibody which is labeled with a fluorophore for visualization binds specifically to the primary antibody (from [16]).

Besides the use of IHC to mark cell types of interest, there are also other methods to stain structures of interest. The most common tissue processing techniques for vasculature visualization in SPIM microscopy are the following ones [17]:

- Immunolabeling of endothelial cell markers on histological sections
- Intravital, intravenous (i.v.) perfusion of an endothelial marker (e.g. tomato-lectin)
- Casting of the vasculature by intravascular injection of a filling agent, followed by corrosion of the surrounding tissue for imaging by scanning electron microscopy (SEM)

2. PROJECT DESCRIPTION

GENERAL EXPERIMENT DESIGN

The motivation of this work is based in the characterization of the vaso-architecture of myocardial infarction and peripheral areas in a mouse heart model using CUBIC and IHC based methods and 3D images of the whole volume acquired with SPIM technology to determine the anatomical characteristics of the microvasculature evolution between acute and chronic infarction.

In Fig. 8 it is visualized the generalized protocol to be followed:

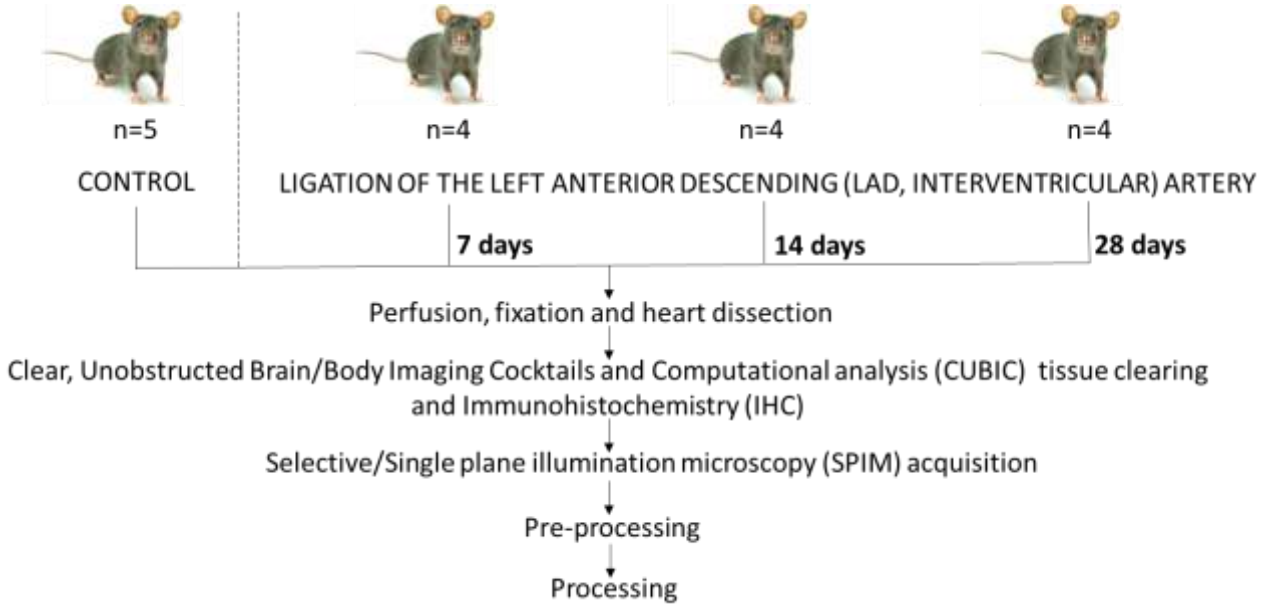

Figure 8. Outline of the experiment protocol.

Firstly, 22 mice were subjected to a ligation of the left anterior descending (LAD) artery surgery in order to induce ischemic condition and MI. Then, 7, 14 and 28 days after this surgical procedure, perfusion and fixation of tissues took place, creating three n=4 groups with different MI chronic stages. Besides, a n=5 slam group was added to be able the comparison with a healthy heart model.

Once the hearts were dissected, they were cleared with CUBIC tissue protocol to allow the deeper light penetration while acquiring images in SPIM microscope and two different approaches to label vasculature were accomplished:

1. Vasculature labelling using IHC technique: a primary antibody (anti-CD31) with a second antibody (Alexa Fluor 647nm).
2. Vasculature labelling by injecting a 649nm Lectin both by intravenous (i.v.) via and while perfusing.

We dyed two of each group with IHC technique and the other two with the Alexa Lectin.

Thenceforward, stack images were acquired with SPIM and pre-processed with some Fiji (ImageJ) [18] plugins or home-written MATLAB® codes to reduce noise, enhance edges and details and remove artifacts produced while acquisition process.

Finally, 4D images are analyzed and processed to measure some changes in vasculature such as total vessel volume, vessel segment number, vessel branch point number, vessel length and vessel diameter.

2.1. OBJECTIVES

- □ Optimization of vasculature labelling method to stain the heart vasculature.
- □ Optimize CUBIC clearing method in order to achieve a good enough whole heart model.
- □ Acquisition of images with different SPIM settings.
- □ Correction of image artifacts and removal of noise produced in the images by developing different home-written codes in MATLAB®.
- □ Processing and analysis of 3D images.

3. MATERIALS AND METHODS

The materials and methods that lead to the results of this work will be explained in detail in this chapter. Firstly, it is explained the animal perfusion and the following fixation of the cardiac tissue. Right after, images were acquired with SPIM. Protocols used are explained along these sections.

3.1. MICE – ETHICS

Male mice, weighting 23.7 to 30.5 g, were divided into 3 groups designated as 7, 14 and 28 days after myocardial infarction is produced. These groups were paired with a fourth one to be used as a control one.

The total number of mice used were 22. There were used 4 mice for each 7, 14 and 28 stages while 5 mice where evaluated as control. The remaining mice died during or due to the ligation of the LAD artery surgery, resulting in a mortality of 20%.

Animal studies were approved by the CNIC Animal Experimentation Ethics Committee and by the Community of Madrid (Ref. PROEX 332/15). All animal procedures conformed to EU Directive 2010/63EU and Recommendation 2007/526/EC regarding the protection of animals used for experimental and other scientific purposes, enforced in Spanish law under Real Decreto 1201/2005.

3.2. LAD – SURGICAL PROCEDURE

The usual model for both acute and chronic MI is the mouse, by ligation the left anterior descending coronary artery (LAD).

Mice were anesthetized and fixed in supine position by tying the legs and the upper jaw. In order to create a simple and fast experimental model of myocardial infarction in mice, a suture is passed from the left fringe of the pulmonary infundibulum to the lower right of the left auricle, with a distance about 2 or 3 mm. The LAD and the great cardiac veins are ligated [19].

All surgical procedures had place in the Centro Nacional de Investigaciones Cardiovasculares Carlos III (CNIC).

3.3. PERFUSION AND FIXATION

The tissue fixation plays a fundamental role in the preparation of the sample. The organs of interest need to be preserved from decay, preventing autolysis and putrefaction [20]. Treating the biological specimen with fixative solutions such as Paraformaldehyde (PFA) stops any on-going biochemical reaction while preserving the proteins and nucleic acids in their place. The process of perfusion and fixation is critical for the labeling of the sample with both lectin and IHC methods. For small biological samples, immersion in the fixative solution (e.g. PFA 4%) is sufficient to diffuse through the whole sample. Nevertheless, often changes in response to hypoxia begin before the tissue can be preserved. For the preservation of intact larger specimens, such as a whole mouse heart, perfusion is needed to effectively deliver the fixative solution to all parts of the tissue.

The advantage of directly perfusing fixative through the circulatory system is that the PFA can quickly reach every corner of the organism through the natural vascular network. In order to utilize the circulatory system most effectively, care must be taken to match physiological pressures [20]. It is important to note that physiological pressures are dependent on the species used. Techniques for perfusion fixation vary depending on the tissue to be fixed and how the tissue will be processed following fixation.

For each n=4 group, 2 rodents were perfused following the conventional protocol and the other 2 were perfused while being labelled with the Alexa Lectin. Both protocols are explained below.

3.3.1. NORMAL PERFUSION PROTOCOL

Two animals from each group (7, 14, 28 and control) and the 5 slam ones were perfused as it is proposed in [22]. All procedures were performed in a ventilated hood since PFA dissolves toxic gases. A previous setup of a peristaltic pump, some surgical instruments, a large bowl and laboratory material was prepared.

The detailed protocol is described below:

1. Animal is deeply anesthetized by injecting 0,3ml of xilane2%-ketamine (1:10) intraperitoneally. Once the animal has reached a surgical state of anesthesia (checked with toe pinch method) the surgery can be undertaken.
2. Using a peristaltic bomb set to a flow rate of 6ml/min, perfuse transcardially through the left ventricle:
   2.1. 15ml of PBS 1x previously warmed for rinsing the blood out of the vessels until the fluid became clear.
   2.2. 30ml of PFA 4% (fixative solution).
3. Dissection of the heart.
4. Post-fixation of the heart in PFA 4% over night at 4°C.

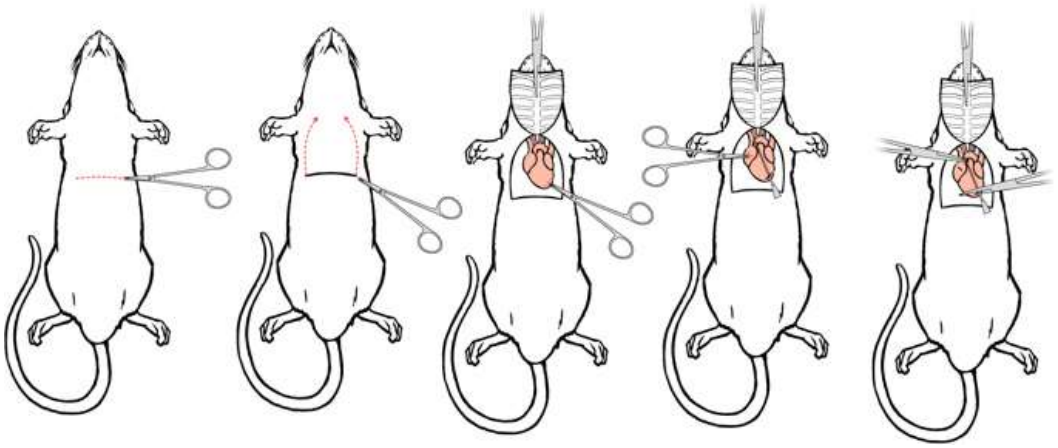

Figure 1. Diagram of perfusion and fixation protocol from [22]

3.3.2. PERFUSION WITH TOMATO LECTIN

In this section, the mice perfusion with lectin from Lycopersicon esculentum (Tomato) to label endothelial cells is described [23]. The detailed protocol for DyLight® 649 lectin perfusion is described below:

1. Animal is deeply anesthetized by injecting 0,3ml of xilane2%-ketamine (1:10) intraperitoneally. Once the animal has reached a surgical state of anesthesia (checked with toe pinch method) the surgery can be undertaken.
2. Injection in cava vein of 0.3ml of Lectin at 10µg/ml (stock at 1mg/ml).

3. Using a peristaltic bomb set to a flow rate of 6ml/min, perfuse transcardially through the left ventricle:
   3.1. 5ml of PBS 1x previously warmed previously mixed with heparin 5U/ml (to avoid blood coagulation) for rinsing the blood out of the vessels until the fluid became clear.
   3.2. 10ml of PFA 1% (fixative solution).
   3.3. 10ml of 649-Lectin at 10µg/ml. Wait 3 minutes to ensure complete vascularization.
   3.4. 30ml of PFA 4%.
4. Dissection of the heart.
5. Post-fixation of the heart in PFA 4% over night at 4°C.

3.4. CUBIC & LABELLING – WHOLE HEART

CUBIC [15] protocol is efficient, simple, easy to apply and reliably compatible with FP fluorescence. These were the reasons to choose this method. Its objectives are:

1. Remove lipids which cause tissue opacity.
2. Homogenize the refractive index within the sample.
3. Preserve the original tissue characteristics and the fluorescence of present fluorophores.

3.4.1. OPTICAL TISSUE CLEARING USING CUBIC PROTOCOL FOR WHOLE MOUSE HEART PROTOCOL

The CUBIC tissue clearing method consist in two reagents called CUBIC-reagent 1 (R1) and CUBIC-reagent 2 (R2). In this work, the protocol period and techniques have been optimized to achieve the tissue clearing of the whole organ.

R1 consist on:

- Urea,
- N,N,N,N-tetrakis(2-hydroxypropyl)ethylenediamine
- Triton X-100
- Distilled water

The urea has the function of solubilizing proteins without denature them. Therefore, the molar concentration of the urea is an important value. With 4.16 M the concentration of the urea is chosen to avoid the proteins from denaturation and leave them in t heir natural configuration. The N,N,N,Ntetrakis(2-hydroxypropyl)ethylenediamine has the function of decolorizing the blood and

solubilizing the tissue. Triton X-100 is a detergent and works as a lipid remover. Lipids are the main reason for light scattering and therefore, they are one of the main causes for tissue opacity [24].

R2 consists on:

- Sucrose
- Urea
- 2,20,20-Nitrilotriethanol
- Distilled water

R2 adjusts the RI of the tissue to approximately 1.48-1.49 [24].

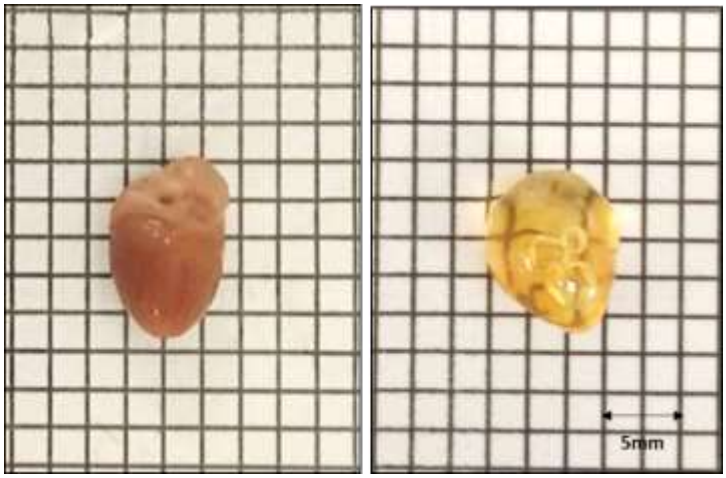

Fig. 12 shows a CUBIC cleared whole mouse heart.

PROTOCOL FOR ANTI-CD31 LABELLING

IHC-method used to label the vasculature is explained in this section.

After perfusion and dissecting the hearts they were embedded in R1 with DAPI (1:2000) following [28] procedure. We implemented the clearing by injecting in the aorta the R1, making possible not only to remove outside lipids but inside ones. R1 and DAPI were changed for fresh every day during the 7 days period. Seven days after the clearing procedure with R1 stops and the sample is washed with PBS with gentle shaking at RT (3 times for 2 h). Primary antibody incubation was carried out incubating the sample in primary antibody solution with anti-CD31 antibody at a concentration of 1:50 and DAPI (1:2000). After 3 days of incubation in the shaker at 37 ±C fresh antibody and DAPI was added. On day 13 of the protocol the incubation with the primary Ab was stopped. The

sample was washed with PBT 0.1% (3 times for 2 h) with gentle shaking at RT. After washing, the incubation with the secondary antibody starts.

The sample was incubated in the secondary antibody solution with the secondary antibody at a concentration of 1:300 and DAPI (1:2000) for seven days. Afterwards, the sample was washed with PBT 0.1% as described above.

Then, the sample was incubated with R2 in the shaker at »80 rpm at 37 ±C for at least 24 h. During the IHC-procedure and the washings the sample becomes opaque again, therefore the transparency of the sample needs to be recovered with the incubation in R2. In Fig. 13 the steps of the protocol are shown.

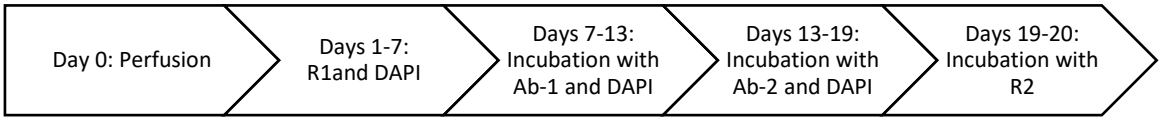

Figure 13. Steps of CUBIC clearing when labelling with anti-CD31

PROTOCOL FOR LECTIN LABELLING

Lectin-method used to label the vasculature is explained in this section.

After perfusion and dissecting the hearts they were embedded in R1 with DAPI (1:2000) following [28] procedure. We implemented the clearing by injecting in the aorta the R1, making possible not only to remove outside lipids but inside ones. R1 and DAPI were changed for fresh every day during the 7 days period. Then, the sample was incubated with R2 in the shaker at »80 rpm at 37 ±C for at least 24 h. During the IHC-procedure and the washings the sample becomes opaque again, therefore the transparency of the sample needs to be recovered with the incubation in R2. In Fig. 14 the steps of the protocol are shown.

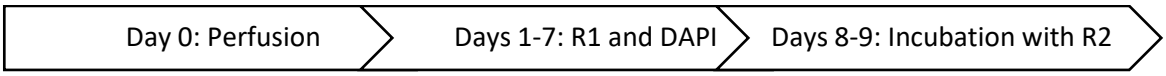

Figure 14. Steps of CUBIC clearing when labelling with lectin

VASO-ARCHITECTURE LABELLING

In this work, we used the first two techniques in order to optimize a labelling technique which allows the complete visualization of the vaso-architecture of the whole organ:

1. Firstly, as a marker for endothelial cells, we used the antibody anti-CD31 (ab28364, Abcam, raised in rabbit) which is expressed on platelets and leukocytes and is primarily concentrated at the borders between endothelial cells (see Fig. 13). As a secondary antibody we used a donkey-anti-rabbit AlexaFluor 647nm (Molecular Probes).

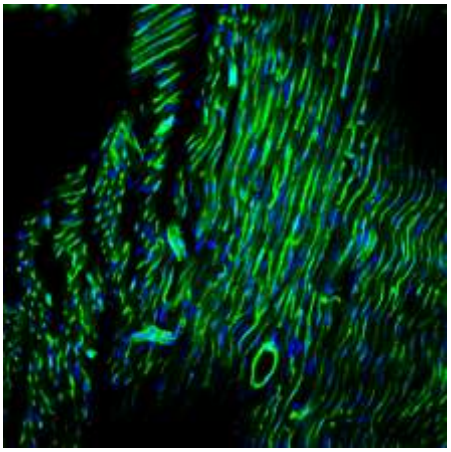

Fig. 13. Anti-CD31 is expressed on platelets and leukocytes and is primarily concentrated at the borders between endothelial cells from confocal microscope.

2. As an alternative approach, instead of staining from outside, we stained the vascular walls from the inside by perfusing an intravascular Tomato lectin dye. Lectins bind specifically at N-acetylglucosamine, which is a derivative of glucose and localized on cell membranes. The injection of lectins has shown to be a marker of all functional blood vessels in rodents [25]. In this work, lectin was injected i.v in the cava vein of the living animal and left for circulation for incubation during 3 minutes [26] and then was introduced during the intracardiac perfusion of the animal [27].

3.4.2. TRANSPARENCY

To measure the cleared organs transparency a set-up with a bright field microscope (Nikon Eclipse E800, Tokyo, Japan) was used. The sample was illuminated with a light source from below and the transmitted light traversing the sample was captured through a Nikon Plan UW2x objective (numerical aperture (NA): 0.06, working distance (WD): 7.5mm) by a

camera (Nikon Digital Camera DXM1200F, Tokyo, Japan) which was mounted above the sample.

Two pictures were taken: one without the sample (see Fig. 14, A) and another one with the sample (see Fig. 14, B). In the image without the sample the light intensity emitted by the light source reached the camera without any disturbance since there was no object in the way: I_0. In the other image the cleared heart is positioned between the light source and the camera and only the light that traversed the cleared sample reached the camera: I. The transparency was calculated with the Lambert-Beer-Law in terms of the attenuation coefficient:

$$I = I_0 e^{-\mu L}$$

Where I is the intensity of the transmitted light through the sample and I_0 is the incident light intensity. μ is the attenuation coefficient in 1/mm and L is the sample thickness that is crossed by the light in its path to the camera. I and I_0 are measured from the image pixel values and the attenuation coefficient is calculated in an implemented Matlab® script.

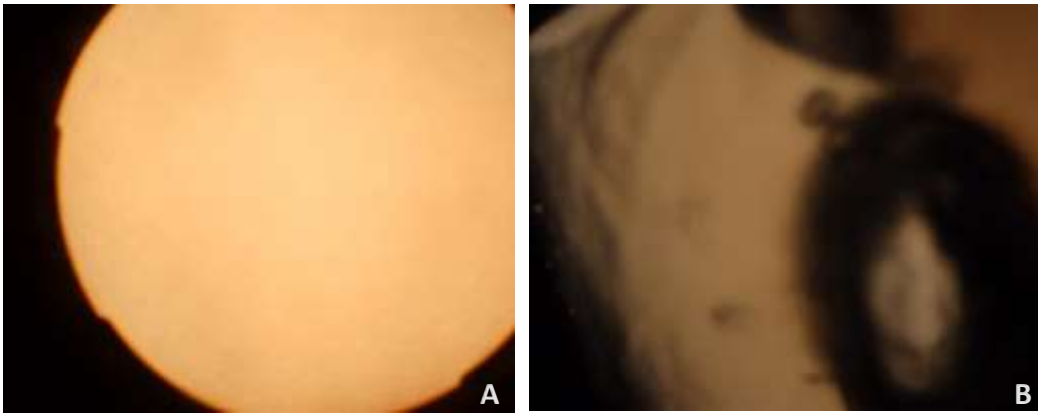

Figure 14. A: without sample. B: with cleared sample

MEASUREMENT OF THE TISSUE TRANSPARENCY

The script needs the manual input of the sample thickness. The first image without the sample is converted into an 8-bit gray scale and visualized on the screen. Three drag able rectangles with 5 % of the image size need to be placed by the user to positions that represent I_0. Off these three rectangles the mean gray value (mean intensity) is calculated by taking the average pixel value and is stored as I_0. The same procedure was carried out with the image where the sample was put into the light path. In this image the user needs to drag the rectangles to positions that represent the tissue and not e.g. shadows or wrinkles in the tissue. These gray values would not be representative for the cleared tissue. The average pixel value of these three rectangles in the sample image is stored as I. Knowing the thickness L of the sample, the attenuation coefficient μ is calculated as:

$$\mu = \frac{-\ln(\frac{I}{I_0})}{L}$$

A high absorption coefficient μ means that lesser light was able to traverse the object which implies that the object remained relatively opaque. The images were taken in three different zones of the object. At the end of the calculations the mean and the standard derivation of the three sample zones and the three calculations of μ were computed.

Transparency was evaluated after 1 day in R1, after 7 days and after R2.

3.5. IMAGE ACQUISITION

In this section the methods which lead to 4D-images in SPIM are described. The final goal is to acquire 4D-images in high resolution of healthy mouse heart tissue and mouse heart tissue that suffered a myocardial infarction in three different stages to quantify changes in the vasculature in the damaged area.

4D-image stacks were acquired with a custom made SPIM at the Medical Imaging Laboratory at Hospital Gregorio Marañón in Madrid. The microscope was built by Dr. Jorge Ripoll of the Universidad Carlos III in Leganés.

3.5.1. SPIM SETUP

The SPIM has five different excitation lasers (Roithner LaserTechnik,Wien, Austria) of varying wavelengths and an assortment of emission filters (Tab. 1). These five lasers allow the use of more than one fluorophore in each sample.

EXCITATION LASSER λ	EMISSION FILTER λ/BANDWIDTH	MATCHING SPECTRA FLUOROPHORES OR DYES
405 nm	475 / 50 nm	DAPI dye
473 nm	531 / 40 nm	AlexaFluor 488, GFP
532 nm	607 / 70 nm	AlexaFluor 555, Cy3 dye
590 nm	700 / 40 nm	AlexaFluor 594, mCherry
635 nm	670 / 10 nm	AlexaFluor 647, Cy5 dye

Table 1. Wavelength pf the excitation lasers with the corresponding emission filters of the SPIM and the corresponding fluorophores used for the five different channels.

The excitation laser is directed through a set of mirrors towards a cylindrical lens that creates the light sheet (see Fig. 15). The illumination objective which is used to direct the laser light sheet into the focal plane is an infinity corrected 5x long working distance objective (Mitutoyo Corporation, Sakado, Japan, NA: 0.14, WD: 34 mm, Depth of focus (DF): 14 μm).

Two infinity corrected long working distance objectives (also Mitutoyo) of three different magnifications are available:

- 2x detection objective: NA: 0.055, WD: 34mm and DF: 91 μm.
- 5x detection objective: NA: 0.42, WD: 34mm and DF: 14 μm.
- 10x detection objective: NA: 0.26, WD: 33.5mm and DF: 3.5μm

The glass tube containing the sample is positioned inside a glass cuvette (Hellma Analytics, Muellheim, Germany) (see Fig. 15). The glass cuvette is filled with oil (Johnson Baby Oil, Johnson & Johnson) for the CUBIC-clearing method. The liquid in the cuvette is used to match the RI of the sample and its immersion medium (see Fig. 16).

The sample is moved by a rotation stage (8MR190-2, Standa, Vilnius, Lithuania) and three motorized stages that allow translation (8MT167-100, Standa). A joystick with three degrees of freedom is used to control the movement of the detection objective (focusing) and the movement towards two of the three translationalmovements (x- and y-direction).

The imaging system consists of a scientific Neo 5.5 sCMOS camera (Andor Corp, Belfast, United Kingdom) which is thermoelectrically cooled to reduce electronic noise.

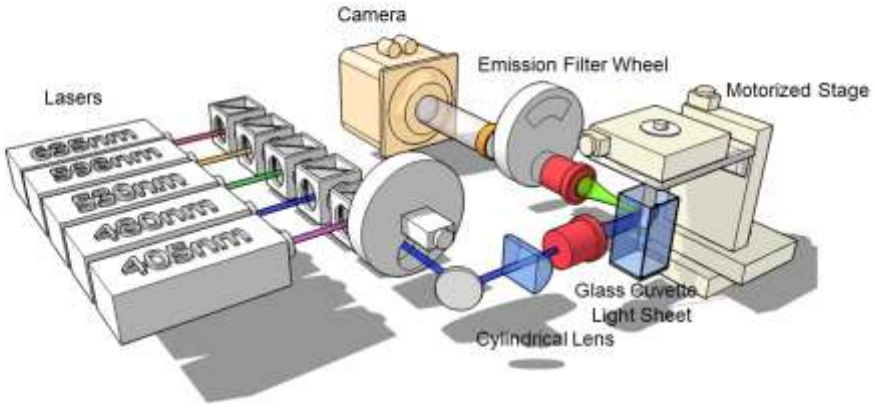

Figure 15: SPIM setup at the Medical Imaging Laboratory. In red: Illumination and detection objectives. The laser is guided with mirrors to the cylindrical lens which forms the light sheet. The light sheet passes the illumination objective and traverses the glass cuvette in which the sample is located. The sample is moved plane by plane (z-direction) with the help of a motorized stage. The emitted light passes through the detection objective and the emission filter and is captured by the camera [Image with permission from Dr. Jorge Ripoll [29]].

The sensor of the camera has 2560 x 2160 active pixels and the physical detector size is 6.5 μm x 6.5 μm. The final image resolution depends on the magnification of the detection objective, the physical size of a camera pixel and on the binning that is used following the formula:

$$ImageVoxelSize = \frac{CameraPixelSize * Binning}{MagnificationObjective}$$

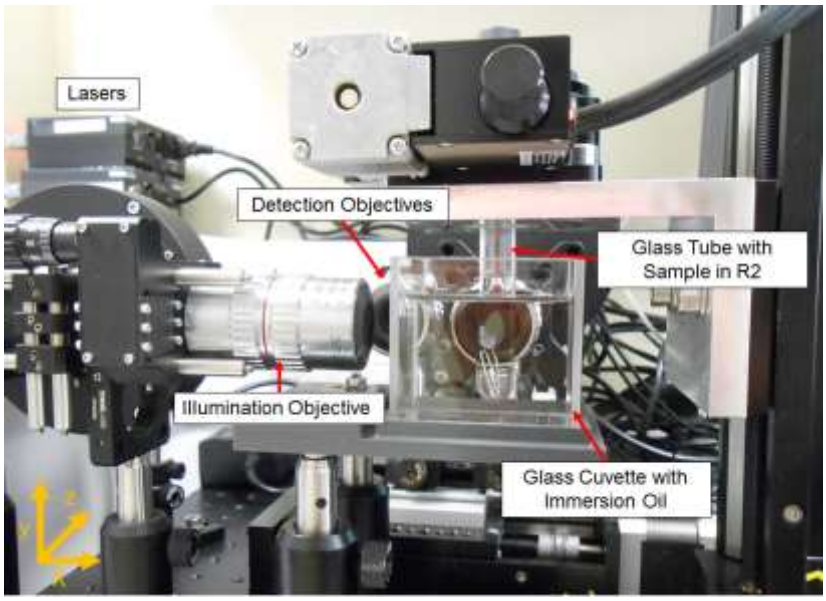

Figure 16: Photograph of the SPIM: Glass cuvette with the immersion oil, illumination and detection objectives, the sample under study immersed in R2 in a glass tube and the excitation lasers. The glass tube with the sample is dipped into the glass cuvette with the immersion oil.

Binning is the merging of two or more adjacent pixels of the sensor in order to achieve faster readout speeds and improved signal to noise ratios at the expense of reduced spatial resolution. Binning of two adjacent pixels was used during the experiments so the final image size was 1280 x 1080 pixels. Using a binning of 2 the image stacks need to be downscaled by factors of 0.5 or 0.25 to reduce the large amounts of data and make the digital processing possible.

3.5.2. IMAGE ACQUISITION WITH SPIM SOFTWARE OPT3D EXPERIMENT

For the image acquisition with SPIM the softwareOpt3D Experiment developed by Dr. Jorge Ripoll was used. The sample can be manually placed into the field of view (FOV) by moving it in the x-, y- and z-direction.

The software allows the programming of excitation laser sequences and their respective emission filters (see Fig. 17 field “Scan List”) and the setting of a series of parameters such as:

- The power of the excitation laser (see Fig. 17, field “Laser”).
- The camera exposure time, which in our experiments varied from 0.2 to 0.5 s (see Fig. 17, field “Live Feed”) depending on the excitation laser, its power and the fluorophore used.
- The initial and final z-positions and the spacing between two consecutive slices of the 3D-image stack, which determines the total number of images to be acquired (see Fig. 17, field “Positioning”).

Figure 17: User Interface for the Opt3D Experiment software to control the SPIM.

The sample is immersed in a cylindrical glass tube filled with R2. The tube is fixed through an accessory component to the moving unit of the microscope and immersed in a static glass cuvette filled with immersion oil. As explained before, the sucrose based R2 was also designed to increase and homogenize the RI of the sample to the RI of the materials and immersion oil used. The IHC-labeled samples present image data in two different channels (excitation/emission wavelengths). One channel for DAPI (nucleus staining) and one for the AlexaFluor secondary antibody (647). The same channel was used for anti-CD31 and lectin perfused hearts. To visualize the DAPI staining the sample was illuminated with the 405 nm laser and the emitted fluorescence signal was collected with a 475 nm emission filter. AlexaFluor 647 fluorochrome and AlexaLectin(649) required the excitation with the 635 nm wavelength laser and signal collection with the 670 nm filter. Because the SPIM has five lasers, the visualization of five different tissue types within the same sample is possible. The detection was performed using the 2x, 5x and 10x magnification objectives. Gray scale images of 16-bit depth were acquired with a binnings of 1 and 2. The spatial resolution is sufficiently high using a binning of 2 while generating a smaller amount of data for 2x and 5x objectives, but it was used the binning 1 with the 10x objective.

The imaged FOV has a size 8.3 mm x 7.0 mm when the 2x objective was used, 3.2mm x 2.8mm when images were acquired with the 5x objective and 1.6 mm x 1.4 mm when the objective used was the 10x. The acquired 3D-image data set is automatically assembled as a TIFF composite stack of all the acquired channels.

3.6. IMAGE PRE-PROCESSING

In this section, the image processing of the 4D-image stacks is described.

Firstly, a noise correction is computed with a home-written Matlab® code to enhance details and edges of vasculature while reducing noise.

Right after, beside the usage of existing software, the implementation of an user interface that corrects the intensity loss of the lasers in the x-direction is described. The rough description of the implemented algorithm is described in [30]. In the following the correction of the stripes artifact in SPIM-images will be described.

3.6.1. IMAGE NOISE CORRECTION

In order to enhance details and edges of vasculature a unsharp masking was applied. This pre-processing of the stacks will facilitate the posterior analysis of the heart vaso-architecture. Moreover, it will also reduce noise present in the acquired images. The algorithm used is based on [35].

The unsharp masking is a morphological transformation which is computed by using a Gaussian filter. The algorithm used in the home-written Matlab® code is explained below. The rough code can be found in the appendix.

Firstly, the directory where the images in .TIFF format are stored is asked to the user. Then, a 3D matrix is created with all slices of the stacks, resulting in the 3D image. A 3D Gaussian filter is applied to that matrix. This step gets a blurred version of the image where the background is blurred and vessel intensities are homogenized. After that, this image is subtracted to twice the original image using Fiji (ImageJ software) [18]. Finally, a new folder is created and each slice is stored in a .TIFF file.

3.6.2. IMAGE ARTIFACTS

The two artifacts that appear due to the acquisition in the SPIM are the presence of stripes and the inhomogeneous illumination along the laser path through the tissue. Both artifacts correction methods are explained below.

3.6.2.1. STRIPES CORRECTION

The stripes artifact occurs due to absorption and scattering of the laser light by objects (e.g. dirt, air bubbles, tissue itself, microscopic dust) in the path of the laser light sheet. This absorption is showed as vertical darker lines in which data is loosed. In Fig. 18 the stripe artifact is demonstrated in a SPIM-image of a mouse heart labelled with DAPI.

Fig 18. Stripes viewed in a DAPI labelled image of heart tissue

As a first approach, the use of *OP3D_Stripes,* a software developed by Prof. Jorge Ripoll, gave us a first result removing these stripes. This software is based on Gabor filter. It removes the stripes by analyzing frequencies contained in the image. But, as the width of the filter is determined by the width of the stripes without having into account de direction, too much information was loosed when vasculature images were processed.

Thus, the stripes artifact in SPIM-images was solved by a home-written implementation in Matlab® of the “rolling ball” algorithm described in [32].

It mainly consists of functions of the mathematical morphology framework. The main operations are a morphological closing followed by a morphological opening operation. The closing operation is a maximum filtering followed by a minimum filtering. This operation is

supposed to close all holes in the intensity graph and to smooth the graph to the background level.

In the first step, the maximum filtering, every pixel is assigned to a new pixel value, namely the maximum of the neighboring n-pixel values. A critical parameter is the parameter “n” of the neighborhood pixels which will become clear later in the paragraph. With this operation holes become filled depending on their size. If a hole is smaller than the n-pixels, it will become filled at the level of the mean intensity. This operation also shifts edges. Therefore, a reverse operation is needed to undo the edge-shifting, which is achieved with the following minimum filtering. This operation smoothes all holes in the intensity graph and fills them with the value of the background level, so the name closing is intuitively clear. If a hole is larger than the filtering element, it is ignored and remains in the intensity graphs. This is the reason why the value of “n” in the structuring element is important and decides which objects are removed and which ones remain in the image. The opening operation is the opposite of the closing operation, where a minimum filtering is followed by a maximum filtering. With this operation small peaks get removed from the image. The opening and closing operations select objects of the intensity graph according to their lateral size independent of the offset or background value. The opening operation followed by a closing-operation is called the “rolling ball” algorithm, because the resulting graph is the line where the surface of a ball with a defined radius is rolling over the intensity graph. Using this operation, the image is smoothed to the background intensity while removing all content from the image. In contrast to the standard linear smoothing techniques, the technique of using morphological filters is not dependent of the absolute intensity values or the difference of brightness values between a fluorophore and background.

Morphological filters smooth everything in the image with a lateral size smaller than the filtering element and gray values do not play a role. The shape of the structuring element defines the content in the image that will be removed. To eliminate the stripes in the images, our structuring element must have a line-shape with its orientation in the same direction as the stripe artifacts in the image. In this way, only vertical content is selectively removed from the image. The structuring element does not “see” vertical changes and

therefore removes everything except the stripes. The resulting image is interpreted as the "local illumination" of every pixel. By pixel-wise dividing the original image by local illumination image and then multiplying every pixel by the mean intensity of the smoothed image, the final stripes artifact corrected image is achieved. The algorithm requires the folder of the .TIFF stack images and creates a new folder with the stripes corrected tiff-stack images. The rough code can be found in the appendix of this work.

3.6.2.2. ILLUMINATION CORRECTION – MATLAB GUIDE

Another standard image artifact is the intensity inhomogeneity, visible along the path of the laser light sheet. Light scattering by the tissue and absorption of the illumination laser light occur and result in intensity inhomogeneity along the light sheet path.

When the excitation laser beam is attenuated as it traverses the sample, less photons reach the sample region located further away from the illumination source, causing an intensity inhomogeneity through the image as well as a decrease in sharpness of that region.

Fig. 19 shows the described effect of the laser beam attenuation along its path while imaging a relatively big sample. As schematized the sample is illuminated by the excitation laser from above. It can be observed that the heart tissue closer to the illumination objective has higher gray values and is sharper while the tissue further away has lower gray values and is blurred, although it is the same tissue and therefore should have the same gray values. Attenuation of the light sheet by scattering in the sample is dependent on the wavelength. According to the Rayleigh scattering phenomenon, the cross section at which light is scattered by particles that are smaller than the incident wavelength, varies inversely with the fourth power of the wavelength (γ^{-4}). This dependence explains why shorter wavelengths (purple and blue light) are scattered more strongly than longer wavelengths (red light).

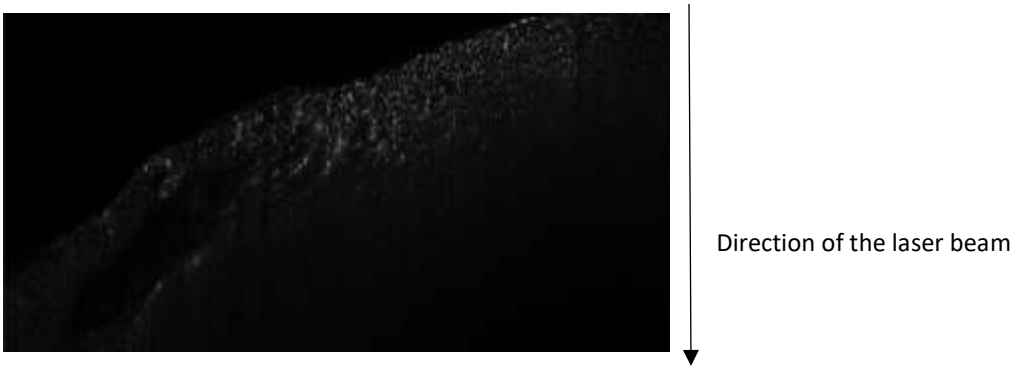

Figure 19. Attenuation oh light due to the scattering caused by the sample. In white, DAPI channel

However, these artifacts need to be corrected before doing any other image processing such as threshold-based segmentation for further quantification methods. Because illumination inhomogeneity is a common problem, there are a lot of attempts and solutions for the correction of these inhomogeneities. Besides the classical work of Sled et al. [33] that consists of filtering MRI-images in the frequency domain with a high-pass filter we found the approach of Schwarz et al. [34] that describes the correction of illumination inhomogeneities in optical images by using the absorption coefficient μ of the tissue. Because in our case the illumination inhomogeneities occur in optical images, we implemented and adapted the described algorithm for image correction [34].

IMPLEMENTATION OF THE ILLUMINATION CORRECTION

The implementation of the illumination correction algorithm was done in Matlab®R2014a. The main idea of the illumination correction described in [34] is the correction of the original with a matrix of correction factors. The correction factors cf in the direction of the light sheet (x-direction) are calculated assuming an exponential attenuation of the excitation and emission light in the tissue.

$$cf_{(\Delta x)} = \frac{1}{e^{(-\mu_x \Delta x)}}$$

The overall structure of the algorithm shown in Fig. 20 containing a flowchart:

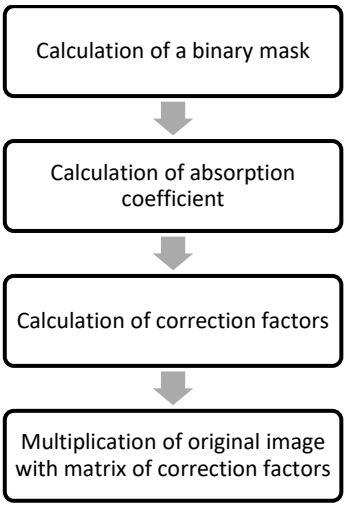

Figure 20: Flowchart of the implemented algorithm correct the inhomogeneity of the illumination laser light.

Step 1:

Two methods were used to calculate a mask for illumination correction. Until this work, the mask was calculated by using the tool "Threshold" of Fiji after subtracting the background. This provided us a global threshold of the image. The obtained mask gave us a good approach for illumination correction of DAPI images but not for vasculature ones as fine detail of vessel edges and damaged zones due to the infarction weren't considered in this correction.

Then, as a second approach we implement a Matlab® code which calculates a local threshold. The rough code can be seen in the appendix. The mask of the .TIFF image stack is calculated in a loop over the whole image stack by using a simple histogram analysis to threshold the images one by one in Fiji tool. First, every image is filtered with a median filter with a 10-times-10 neighbourhood to smooth the image and remove noise. Then the highest peak in the histogram is found is a value of the background. The threshold to calculate the binary mask is set to the grey value of the peak analysis and an additive 10 % containing also brighter background values and thus being a security margin. So, every grey value higher than the threshold value is set to 1 and every value lower to 0.

Step 2:

We calculate the absorption coefficient μ according to Beer-Lambert Law, following:

$$I = I_0 e^{-\mu l}$$

We take one image of the whole 3D-image stack at 1/4, one at 1/2 and one at 3/4 of the stack size in z, to keep the calculation time and user interactions to a minimum. For each image we take the mean intensity values of two rectangular regions. These two rectangular regions, that have 5 % of the image size in x and y, can either be placed manually by the user or the regions could be calculated automatically. For the automatic placing of the rectangles we calculate the middle of the object mask and find the first and last row of the mask. With a security margin of half of the rectangle size in the y-direction the rectangles get placed centrally on the upper and lower margin of the object. In the case of the manual setting of the rectangles the user needs to place the first rectangle in the uppermost part of the image (into the sample, not into the background), where the laser still has its full power. The second rectangle needs to be placed in the region, where the light sheet exits the sample and the tissue can barely be seen by the user because of the much lower grey values due to the intensity loss of the laser by light scattering and absorption in the tissue.

Step 3:

For each image of the 3D-stack the matrix with the correction factors defined in

$$cf_{(\Delta x)} = \frac{1}{e^{(-\mu_s \Delta x)}}$$

is calculated.

Step 4:

In the last step the Gaussian blurred object mask is multiplied with the correction factor matrix and finally the original image is stored in a new folder file.

All these steps were included in a Matlab® GUI user interface as it is shown in Fig. 21.

Figure 21: Final steps of the illumination correction algorithm. The original image on the left is multiplied with the mask of the image and the correction factor matrix. The output image is the illumination corrected image.

The user interface was implemented to provide the user the setting of changing the contrast window and level resolution, to move along the image stack and to rotate the image. The code was included in the appendix.

3.8. DATA ANALYSIS

Following to the pre-processing step, the parameters to be evaluated between healthy and 7, 14 and 28 days post-myocardial infarction occurred are: total vessel volume, vessel segment number, vessel branch point number, vessel length and vessel diameter.

To do that, different tools are going to be used.

Images have been normalized by using the 2 and 98 quartiles with an easy and fast home-written Matlab® code. These values were chosen as minimum and maximum leaving a margin of error to avoid taking as a global maximum a noise pixel. The normalization ensured the homogeneous illumination along x-path in the stack (between slices) and it provided the viability to compare images with different width.

3.8.1. Fiji

Fiji (ImageJ) software provides the tool to skeletonize in the plugin “3D Skelotonize”. It converts the image into a network graph. The branching points are identified (raw skeleton) and then iteratively short or false vessel segments are removed. Then, measurements are taken by Euclidean distances as in [22].

3.8.2. 3D SLICER

3D Slicer is an open source software platform for medical image informatics, image processing, and three-dimensional visualization [31]. It provides the 3D visualization of the processed images and the creation of videos and renderings of the resulting stacks.

4. RESULTS

In this last chapter results obtained from all methods explained above are shown.

4.1. CUBIC, IHC and SPIM

Upon macroscopic observation, the infarcted region should be seen off-white. Myocardium of the anterior wall of the left ventricle and of the apex of the heart, around suture, was indeed off-white (Fig. 22). Dilation of the left ventricle and thinness of the ventricular wall were also found in these specimens (Fig. 23).

In the left ventricular wall, necrosis was found in most of the myocardium and in the papillary muscle. The cardiac muscle fiber became thin. A few remnant cardiac muscle cells were found only in the endocardium and the epicardium.

As it was expected, more damaged walls and necrotic areas appeared when myocardial infarction was chronic (28 days). In addition, 28 hearts acquire strong differences in morphology.

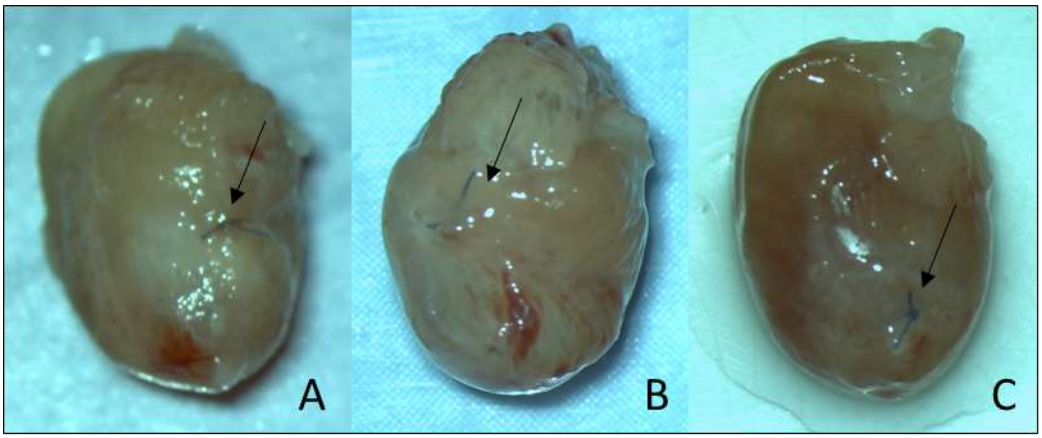

Figure 22. Arrow points towards the suture location in 7 (A), 14 (B) and 28 (C) infarcted models. The anterior wall of the left ventricle and the apex of the heart were off-white and bulged outward.

Figure 23. Arrow points toward the area where the wall is thinner due to the MI

The transparency analysis after the CUBIC tissue clearing showed a successful method as the whole organ results to be cleared (as it was shown in Fig. 12) and measurements in the optical microscopy proved it. Statistics results are shown in the table below.

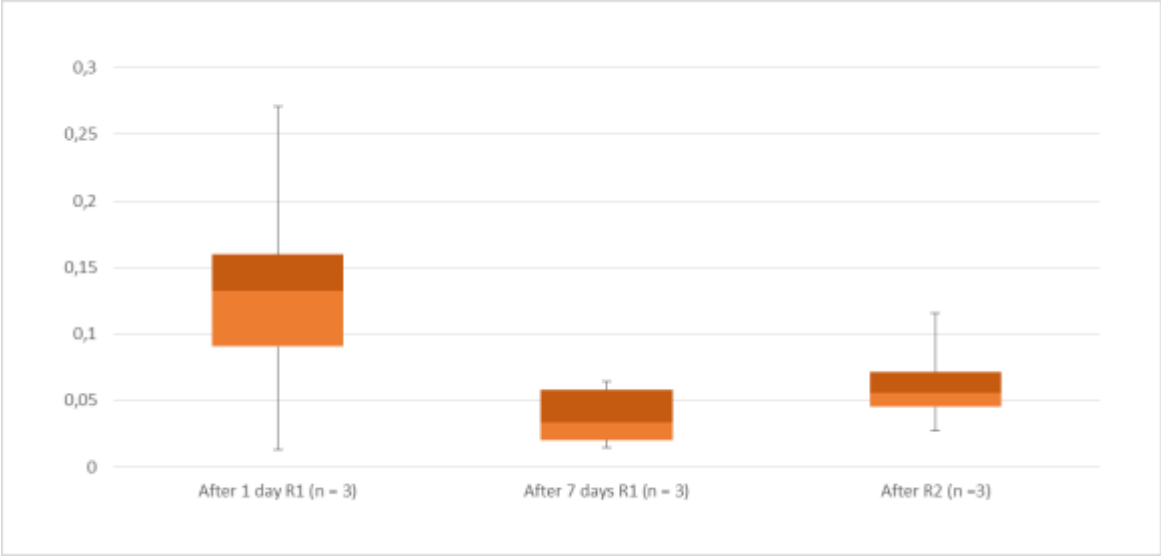

Table 2. Analysis of transparency achieved by CUBIC clearing by embedding the sample and injecting R1 by aorta vessel

The implementation of injecting R1 by the aorta not only enhances the clearing but it also provides a better visualization of vasculature labelling while SPIM images acquisition.

The i.v. staining with Lectin showed much better results than anti-CD31 in deeper structures of the heart. Then, all posterior analysis of images was computed with Lectin labelled samples.

4.2. SPIM ACQUISITION AND PRE-PROCESSING

The suture of the myocardial infarction could be for the very first time easily localized inside the whole heart sample thanks to SPIM techniques (see Fig. 24).

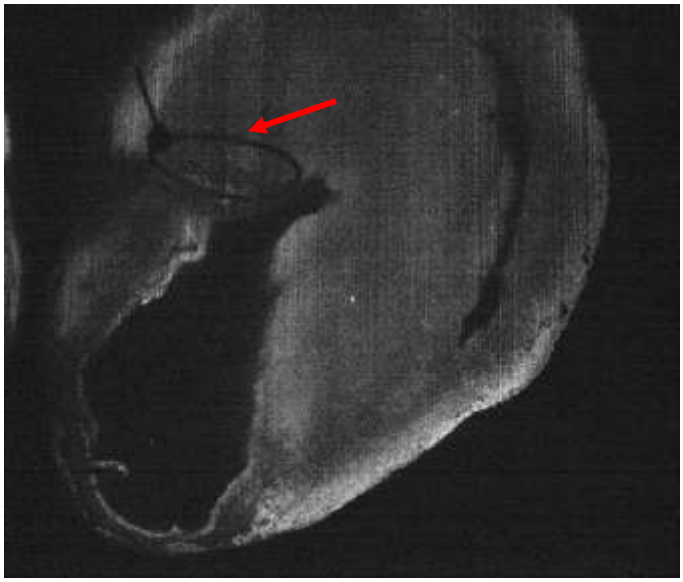

Fig. 24. Whole DAPI labelled image acquired with 2x objective of SPIM. Red arrow points toward the suture which caused the MI in a 7 days stage heart. Blue arrow points toward the infarcted area.

Hereunder, the complete pre-processing of an 5x Lectin labelled SPIM image is showed:

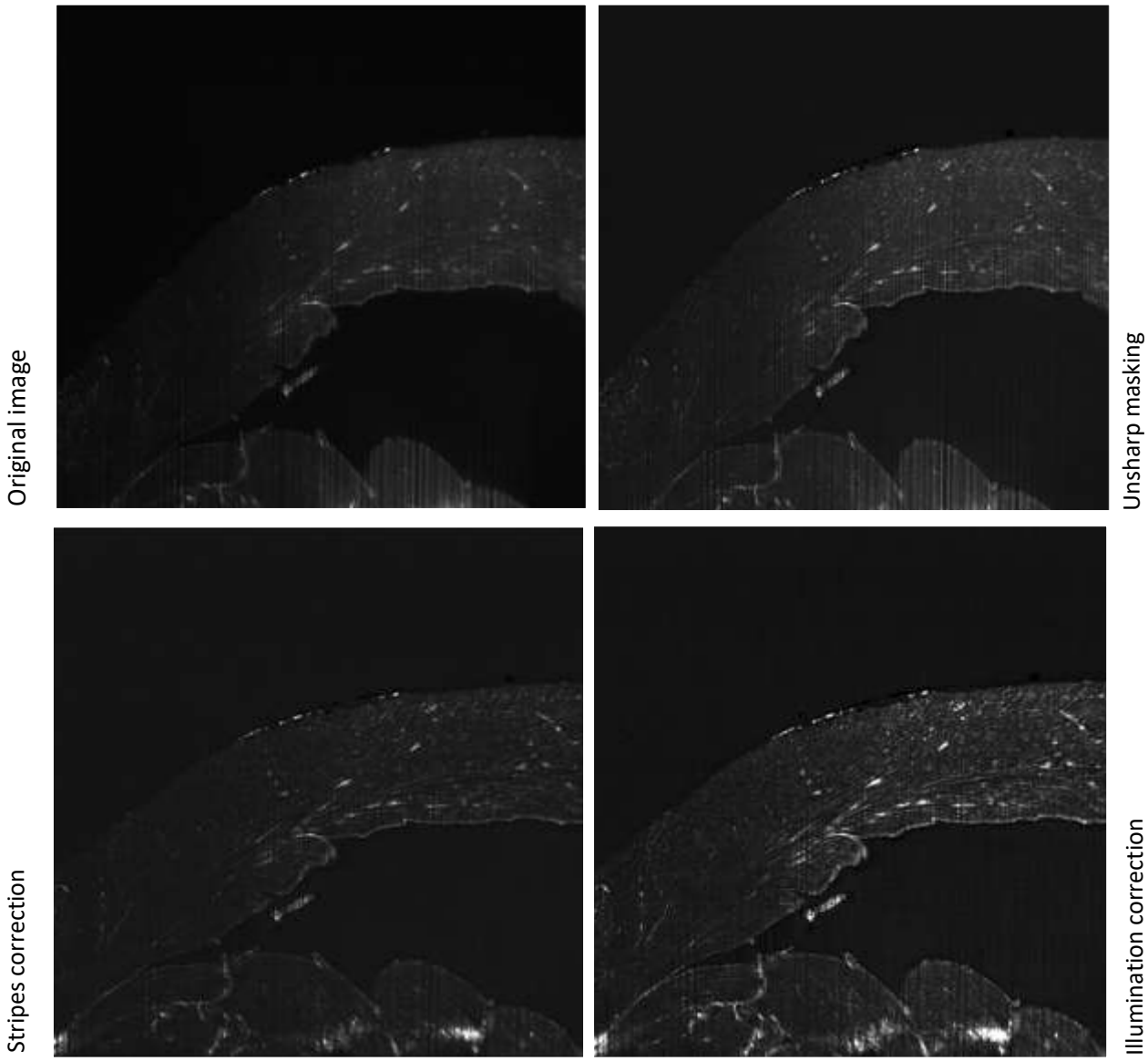

Figure 25. Pre-processing steps to acquire the image to be analyzed

Once the stacks have been pre-processed we proceed to the analysis. In Fig. 26 the 3D volume can be visualized by using 3D slicer software.

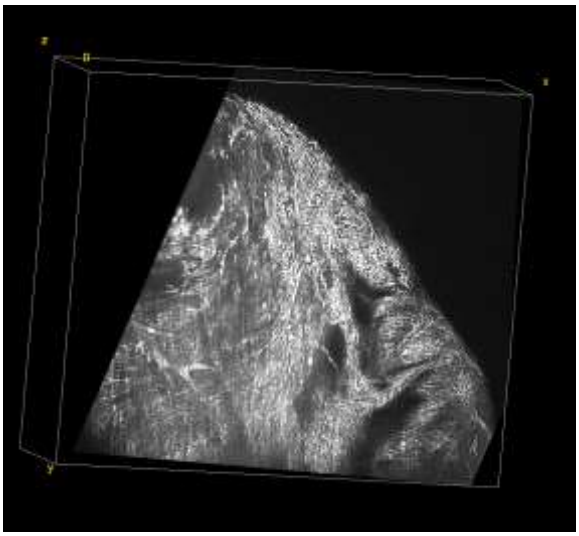

Fig. 26. 3D image from a rendering of apex region of the heart acquired with the 5x objective by SPIM.

Since the stripes correction provided not good enough results, the analysis of images didn't give us accurate results. As a solution, we proposed a collaboration with Prof. Mónica Abella in which we are now working. The goal is the implementation of an algorithm created for correcting ring artifact present in CT acquisition.

Concurrently, we are working in collaboration with Polyxenia Gkontra of CNIC. She belongs to the investigation group of A. G. Arroyo. They are studying parallelly the MI in small pieces of pig tissue by evaluating with fractals the fractal dimension, the lacunarity and the succolarity [36].

5. CONCLUSIONS AND DISCUSSION

This project had the goal to compare the vaso-architecture of a healthy heart with the affected myocardial infarction hearts after 7, 14 and 28 days. For that, it was necessary to establish a method to stain the mouse heart vasculature and render possible 3D-visualization of the vascular network using Single Plane Illumination Microscopy. Eventually, with this new method we will quantify the micro- and macrovasculature to make visible the vascular changes in the myocardial infarction area. Also, other diseases with pathological changes in the vasculature could be studied more in detail with this method that enables the visualization of the vasculature or certain protein distributions in cellular 3D-resolution.

CLEARING OF THE MOUSE HEART AND LABELLING METHODS

A clearing and labelling protocol for the mouse heart has been optimized in our laboratory.

The performance of the CUBIC-clearing technique for the mouse heart model used in this project was assessed through transparency measurement which is, from now on, used routinely for every sample.

We optimized the incubation periods to minimize the tissue processing times while achieving the desirable transparency. In [37] Kolesová et al. show that the best transparency in mouse hearts is achieved with applying the CUBIC-clearing protocol in comparison with other clearing methods.

The best transparency is achieved with the incubation only in CUBIC-reagent 1. Moreover, the implementation of injecting R1 by the aorta helped to achieve the whole organ clearing. Nevertheless, for SPIM-imaging samples that are immersed in R1 also the cuvette of the SPIM needs to be filled with R1 to match the RIs rather than with immersion oil. This is a disadvantage, because R1 is very inhomogeneous and leads to imaging artifacts that do not occur when samples are immersed in R2 and the cuvette is filled with the RI matching immersion oil. The solution to this problem would be to incubate the samples in R2 with a little decline in transparency.

To study the distribution of the micro- and macrovasculature involved in heart infarction labelling protocols for fluorescence microscopy were successfully performed in the whole cleared mouse hearts. Since the Ab does not seem to penetrate into the whole tissue we selected as best labelling technique the Alexa Lectin injection i.v.. Given the fact that the heart is a muscle and a very firm tissue we concluded that the Ab does not succeed to diffuse deeper into the myocardium.

Other combinations of fluorophore-lectin conjunctions with more photo stable fluorophores could be tested in future experiments. In [21] Jährlich et al. use "Ultramicroscopy" to visualize FITC-lectin labeled vascular networks. The advantage of using UM rather than SPIM is, that the sample gets illuminated with two lasers, one on each side of the sample. They therefore achieve a better resolution in the x-direction due to the reduction of the blurring effect produced by light scattering. Nevertheless, until now quantification approaches have not been carried out and also the Alexa lectin labeled auricles of the heart and not the ventricles have been presented. Because of the anatomical location of a myocardial infarction we were interested in labeling and quantifying the apical area of the heart and the labelling results achieve enough depth.

3D-IMAGING IN CUBIC-CLEARED HEART TISSUE

The protocols of 3D-imaging of CUBIC-cleared samples in confocal microscopy with the

IHC- and Alexa-lectin labeling methods were optimized.

Clearing the samples enhances the ability of the Ab to enter into the thick tissue sections through solubilizing the tissue. Simultaneously, clearing the tissue also enables the laser to enter deeper into the tissue and thus, making 3D-imaging with highest resolution possible. In [17] Dickie et al. label vascular networks via intravital i.v. injection of diluted Alexa lectin solution. They achieve 3D-image stacks of up to 1500 µm in confocal microscopy. In confocal microscopy the imaging depth is limited by the working distance of the magnification objective, so the differences in these results compared with ours can be explained by the different disposition of imaging objectives.

In SPIM the protocols for vascular labeling combined with long clearing protocols need to be further optimized. To enable the quantification of micro- and macrovasculature in a large field of view and in 3D other clearing methods like iDISCO [13] or CLARITY [14] could be tested. Some of them are available in our laboratory.

Although the perfusion with FITC-lectin is more cost efficient to achieve vascular staining, it would also be interesting to try IHC-methods with small pieces of tissue in combination with SPIM-imaging. The incubation with antibodies allows the labeling of several antigens at the same time and therefore would exploit the full capacity of SPIM.

IMAGE PROCESSING

The stripes artifact can be removed using the implemented version of the rolling ball algorithm for SPIM-images. Although image information in terms of sharpness and resolution is lost, the decision if the procedure of stripes removal is necessary and would improve the image needs to be made for every single sample. Thus, we are working in collaboration with Mónica Abella to enhance this correction. The implementation of this step would be tricky in order to achieve a good analysis of vasculature.

The most efficient way to obtain high quality images without artifacts however, is good and clean tissue manipulation. Avoiding air bubbles can be achieved through the repose of the sample in R2, so air bubbles have time to rise to the surface before imaging with SPIM. As the heart is a hole muscle, air bubbles can also be located in its interior. We removed them by injecting R2 by the aorta. Also, the immersion oil in the cuvette needs to be changed or filtered for dust and dirt particles at least biweekly. In general, the occurrence of objects that disturb the laser light sheet in its way need to be prevented.

The implemented algorithm for the correction of the inhomogeneous illumination is very useful. Without the prior correction of the inhomogeneous illumination, further segmentation methods would surely not work. The methods would not work correctly due to the large variations in the gray values even though being the same tissue.

6. PROJECT COSTS

The budget for this project was estimated taking into account three types of resources: human resources, laboratory material and technical equipment.

HUMAN RESOURCES COSTS

Human resources costs comprise the salaries of the team members of the project.

Human resources	Cost/Hour	Working Hours	Total Cost
Project Manager/PI	€35	400	€14,000
Student	€25	970	€24,250
			€38,250

Table 3.Human Resources Costs

TECHNICAL EQUIPMENT COSTS

Technical equipment costs include laboratory machinery and the different software and the computer hardware used. Other laboratory equipment includes small everyday use instruments such as the magnetic stirrer, the precision weighting balance, the Vortex mixer, etc.

Equipment	Average life time in years	Unit cost	Units	Depreciation per month	Months employed	Total cost
SPIM	10	€120,000	1	€ 1,000.0	4	€4,000.00
SPIM software license	1	€1,000	1	€83.33	4	€333.32
Image J software		€0	1	€0.00	8	€0.00

Matlab software license	1	€2,000	1	€166.66	8	€999.96
Office 2010 license	2	€139	1	€5.80	8	€46.40
Personal computer	5	€700	1	€10.00	8	€80.00
Shaker	5	€5,000	1	€83.33	8	€666.64
Other laboratory devices	5	€4,500	1	€75.00	8	€600.00
						€6,773.28

Table 4. Technical Equipment associated costs

LABORATORY MATERIAL COSTS

Costs of laboratory material includes all reagents and IHC antibodies, as well as expendable material. Expendable laboratory material includes everyday items used such as Falcon tubes, Pasteur pipettes, multiwall culture plates, etc. This material is supplied directly at the Hospital and during the project we acquired eight packs containing different items, as needed. The approximate cost of each order was 30€.

Laboratory Material	Units	Cost/Unit	Total Cost
Clearing Reagents	1	€400	€400
Laboratory Reagents	1	€500	€500
IHC Primary Antibodies	1	€250	€250

IHC Secondary Antibodies	1	€100	€100
Alexa Lectin 649	1	€750	€750
Expendable laboratory material	8	€30	€240
			€2240

Table 5.Laboratory Material associated costs

7. BIBLIOGRAPHY

[1] "The top 10 causes of death", *World Health Organization*, 2017. [Online]. Available: http://www.who.int/mediacentre/factsheets/fs310/en/. [Accessed: 26- Sep- 2017].

[2] G. Tortora and B. Derrickson, *Principles of Anatomy and Physiology, 13th Edition, 2-Volume Set, Internati*. John Wiley & Sons, 2011.

[3] F. Pampaloni, B. Chang and E. Stelzer, "Light sheet-based fluorescence microscopy (LSFM) for the quantitative imaging of cells and tissues", *Cell and Tissue Research*, vol. 360, no. 1, pp. 129-141, 2015.

[4] "Introduction to Fluorescence Microscopy", *Nikon's MicroscopyU*, 2017. [Online]. Available: http://www.microscopyu.com/articles/fluorescence/fluorescenceintro.html. [Accessed: 26- Sep- 2017].

[5] R. Steiner, "Principles of fluorescence spectroscopy", *Analytical Biochemistry*, vol. 137, no. 2, p. 539, 1984.

[6] "The Fluorescence Microscope", *Nobelprize.org*, 2017. [Online]. Available: http://www.nobelprize.org/educational/physics/microscopes/fluorescence/. [Accessed: 26- Sep- 2017].

[7] H. Ishikawa-Ankerhold, R. Ankerhold and G. Drummen, "Advanced Fluorescence Microscopy Techniques—FRAP, FLIP, FLAP, FRET and FLIM", *Molecules*, vol. 17, no. 12, pp. 4047-4132, 2012.

[8] S.L. Jacques, "Optical properties of biological tissues", Physics in Medicine and Biology, vol. 58, no11, 2013.

[9] D.A. Yushchenko and C.Schultz, "Tissue clearing for optical anatomy", Angewandte Chemie, vol. 52, no. 42, pp. 10949-10951, 2013.

[10] H. Hama, H. Kurokawa, H. Kawano, R. Ando, T. Shimogori, H. Noda, K. Fukami, A. Sakaue-Sawano, and A.Miyawaki, "Scale: a chemical approach for fluorescence imaging and reconstruction of transparent mouse brain," *Nature Neuroscience*, no. 14, pp. 1481–1488, 2011.

[11] K. Becker, N. Jaehrling, S. Saghafi, R. Weiler, H.-U. Dodt, and M. G. Tansey, "Chemical clearing and dehydration of gfp expressing mouse brains," *PLoS One*, vol. 7, no. 3, 2012.

[12] M.-T. Ke, S. Fujimoto, and T. Imai, "Seedb: a simple and morphology-preserving optical clearing agent for neuronal circuit reconstruction," *Nature Neuroscience*, vol. 16, pp. 1154–1161, 2013.

[13] N. Renier, Z.Wu, D. J. Simon, J. Yang, P. Ariel, andM. Tessier-Lavigne, "idisco: a simple, rapid method to immunolabel large tissue samples for volume imaging," *Cell*, vol. 159, no. 4, pp. 896–910, 2014.

[14] K. Chung, J.Wallace, S.-Y. Kim, Sandhiya, A. S. Andalman, T. J. Davidson, J. J.Mirzabekov, K. A. Zalocusky, J.Mattis, A. K. Denisin, S. Pak, H. Bernstein, C. Ramakrishnan, L. Grosenick, V. Gradinaru, and K. Deisseroth, "Structural and molecular interrogation of intact biological systems," *Nature*, vol. 497, pp. 332–337, 2013.

[15] E. A. Susaki, K. Tainaka, D. Perrin, H. Yukinaga, A. Kuno, and H. R. Ueda, "Advanced cubic protocols for whole-brain and whole-body clearing and imaging," *Nature Protocols*, vol. 10, pp. 1709–1727, 2015.

[16] D.Munch, "Schematic diagram of primary and secondary antibody binding. wikipedia, 2007." https://en.wikipedia.org/wiki/File:Primary-Secondaryantibody.svg. [Accessed: 26- Sep- 2017].

[17] R. Dickie, R. Bachoob, M. Rupnickc, S. Dallabridac, G. DeLoida, J. Laia, R. DePinhoe, and R. Rogersa, "Three-dimensional visualization of microvessel architecture of whole-

mount tissue by confocal microscopy", *Microvascular Research*, vol. 72, no. 1, pp. 20–26, 2006.

[18] Schindelin, J., Arganda-Carreras, I., Frise, E., Kaynig, V., Longair, M., Pietzsch, T., … Cardona, A. (2012). Fiji: an open-source platform for biological-image analysis. *Nature Methods*, *9*(7), 676–682.

[19] Wang, J., Bo, H., Meng, X., Wu, Y., Bao, Y., & Li, Y. (2006). A simple and fast experimental model of myocardial infarction in the mouse. Texas Heart Institute Journal, 33(3), 290–3. Retrieved from http://www.ncbi.nlm.nih.gov/pubmed/17041683%5Cn

[20] G. J. Gage, D. R. Kipke, andW. Shain, "Whole animal perfusion fixation for rodents," *Journal of Visualized Experiments*, vol. 65, 2012.

[21] N. Jährling, K. Becker, and H.-U. Dodt, "3d-reconstruction of blood vessels by ultramicroscopy," Organogenesis, vol. 5, no. 4, pp. 227–230, 2009.

[22] Susaki, E. A., Tainaka, K., Perrin, D., Yukinaga, H., Kuno, A., & Ueda, H. R. (2015). Advanced CUBIC protocols for whole-brain and whole-body clearing and imaging. Nature Protocols, 10(11), 1709–1727. [23] "3d-reconstruction of blood vessels by ultramicroscopy"

[24] E. A. Susaki, K. Tainaka, D. Perrin, F. Kishino, T. Tawara, T. M. Watanabe, C. Yokoyama, H. Onoe, M. Eguchi, S. Yamaguchi, T. Abe, H. Kiyonari, Y. Shimizu, A. Miyawaki, H. Yokota, and H. R. Ueda, "Whole-brain imaging with single-cell resolution using chemical cocktails and computational analysis," *Cell*, vol. 157, pp. 726–739, 2014.

[25] S.Mazzetti, S. Frigerio,M. Gelati, A. Salmaggi, and L. Vitellaro-Zuccarello, "Lycopersicon esculentum lectin: an effective and versatile endothelialmarker of normal and tumoral blood vessels in the central nervous system," *European Journal of Histochemistry*, vol. 48, no. 4, pp. 423–8, 2004.

[26] R. Dickie, R. Bachoob, M. Rupnickc, S. Dallabridac, G. DeLoida, J. Laia, R. DePinhoe, and R. Rogersa, "Three-dimensional visualization ofmicrovessel architecture of whole-mount tissue by confocal microscopy," *Microvascular Research*, vol. 72, no. 1, pp. 20–26, 2006.

[27] N. Jährling, K. Becker, and H.-U. Dodt, "3d-reconstruction of blood vessels by ultramicroscopy," *Organogenesis*, vol. 5, no. 4, pp. 227–230, 2009.

[28] Nehrhoff, I., Ripoll, J., Samaniego, R., Desco, M., & Gómez-Gaviro, M. V. (2017). Looking inside the heart: a see-through view of the vascular tree. Biomedical Optics Express, 8(6), 3110. http://doi.org/10.1364/BOE.8.003110

[29] B. Zufiria, D. I. Bocancea,M. V. Gómez-Gaviro, J. J. Vaquero, M. Desco, M. Fresno, J. Ripoll, and A. Arranz, "3d imaging of the cleared intact murine colon with light sheet microscopy," *SPIE Proceedings, Three-Dimensional and Multidimensional Microscopy: Image Acquisition and Processing XXIII*, vol. 9713, 2016.

[30] M. K. Schwarz, A. Scherbarth, R. Sprengel, J. Engelhardt, P. Theer, and G. Giese, "Fluorescent-protein stabilization and highresolution imaging of cleared, intact mouse brains," *PLoS ONE*, vol. 10, no. 5, 2015.

[31]3D Slicer. (2017). Slicer.org. From https://www.slicer.org/. [Accessed: 26- Sep- 2017].

[32] U. Leischner, A. Schierloh, W. Zieglgaensberger, and H.-U. Dodt, "Formalin-induced fluorescence reveals cell shape and morphology in biological tissue samples," *PLoS ONE*, vol. 5, no. 4, 2010.

[33] J. G. Sled, A. P. Zijdenbos, and A. C. Evans, "A nonparametric method for automatic correction of intensity nonuniformity in mri data," *IEEE Transactions OnMedical Imaging*, vol. 17, no. 5, pp. 87–97, 1998.

[34] M. K. Schwarz, A. Scherbarth, R. Sprengel, J. Engelhardt, P. Theer, and G. Giese, "Fluorescent-protein stabilization and highresolution imaging of cleared, intact mouse brains," *PLoS ONE*, vol. 10, no. 5, 2015.

[35] Poplawsky, A. J., Fukuda, M., Kang, B. man, Kim, J. H., Suh, M., & Kim, S. G. (2017). Dominance of layer-specific microvessel dilation in contrast-enhanced high-resolution fMRI: Comparison between hemodynamic spread and vascular architecture with CLARITY. NeuroImage.

[36] Gkontra, P., Żak, M. M., Norton, K. A., Santos, A., Popel, A. S., & Arroyo, A. G. (2015). A 3D fractal-based approach towards understanding changes in the infarcted heart microvasculature. In Lecture Notes in Computer Science (including subseries Lecture Notes in Artificial Intelligence and Lecture Notes in Bioinformatics) (Vol. 9351, pp. 173–180).

[37] H. Kolesova, M. Capek, B. Radochova, J. Janacek, and D. Sedmera, "Comparison of different tissue clearing methods and 3d imaging techniques for visualization of gfp-expressing mouse embryos and embryonic hearts," Histochemistry and Cell Biology, vol. 146, no. 2, pp. 141–152, 2016.

APPENDIX

HOME-WRITTEN MATLAB ® CODES

```
%%UNSHARP MASKING CODE

%Ask for image stack directory
directory_image =uigetdir('C:\','Select directory:');

srcFiles = dir(strcat(directory_image,'\*.tif'));  %struct which store
data
%about image stack directory
for i = 1 : length(srcFiles)
    filename = strcat(directory_image,'\',srcFiles(i).name);
    I = imread(filename);
    img(:,:,i) = I; %img is the 3D image
end

size_img=size(img);
% figure, imshow(img(:,:,ceil(size_img(3)/2)),[]), title('Original
image')
%to show the middle slice of the stack
img = squeeze(img); %it removes singleton dimensions


sigma=2;        %Standard deviation of the Gaussian distribution,
specified
%as a numeric, it refers to FWHM
%size of the filter: 2*ceil(2*sigma)+1 (default)
imgSmooth = imgaussfilt3(img, sigma); %a Gaussian 3D filter is applied

% figure, imshow(imgSmooth(:,:,ceil(size_img(3)/2)),[])  %shows middle
% slice after gaussian
% title('Gaussian filtered image')

filtered_img=2*img-imgSmooth;   %unsharp masking to highligh fine
detail
% figure, imshow(filtered_img(:,:,ceil(size_img(3)/2)),[]) %shows
middle
% slice after sustracting smooth version

%Save in a new directory:
directory_out_img = strcat(directory_image,'_filtered');

if ~isdir(directory_out_img)
    mkdir(directory_out_img);
end


for j = 1 : size_img(3)
    savename= fullfile(directory_out_img,srcFiles(j).name);
    imwrite(uint16(filtered_img(:,:,j)), savename);
end
```

```
%%STRIPES CORRECTION CODE

function [ result_img ] = stripe_remove( img_original, n)

img_inv = imcomplement(img_original);
% function [ result_img ] = stripe_remove( img_original, dist )
% illumination_image =
imopen(imclose(img_inv,strel('line',dist,90)),strel('line',dist,90));


%stripes must be in vertical direction

% 1. Closing
closed_img = imclose(img_inv,strel('line',n,90));
% 2. Opening
morf_img= imopen(closed_img,strel('line',n,90));

%SE = strel('line',LEN,DEG) creates a flat linear structuring element
%     that is symmetric with respect to the neighborhood center. DEG
%     specifies the angle (in degrees) of the line as measured in a
%     counterclockwise direction from the horizontal axis. LEN is
%     approximately the distance between the centers of the structuring
%     element members at opposite ends of the line.

% avg = mean2(illumination_image);
avg=mean2(morf_img);

% result_img_inv =
uint16((double(img_inv)./double(illumination_image)).*avg);
result_img_inv = uint16((double(img_inv)./double(morf_img)).*avg);
result_img = imcomplement(result_img_inv);

end
```

```
%%UNSHARP MASKING CODE

%Ask for image stack directory
directory_image =uigetdir('C:\','Select directory:');

srcFiles = dir(strcat(directory_image,'\*.tif'));  %struct which store
data
%about image stack directory
for i = 1 : length(srcFiles)
    filename = strcat(directory_image,'\',srcFiles(i).name);
    I = imread(filename);
    img(:,:,i) = I; %img is the 3D image
end
```

```
size_img=size(img);
% figure, imshow(img(:,:,ceil(size_img(3)/2)),[]), title('Original
image')
%to show the middle slice of the stack
img = squeeze(img); %it removes singleton dimensions


sigma=2;        %Standard deviation of the Gaussian distribution,
specified
%as a numeric, it refers to FWHM
%size of the filter: 2*ceil(2*sigma)+1 (default)
imgSmooth = imgaussfilt3(img, sigma); %a Gaussian 3D filter is applied

% figure, imshow(imgSmooth(:,:,ceil(size_img(3)/2)),[])  %shows middle
% slice after gaussian
% title('Gaussian filtered image')

filtered_img=2*img-imgSmooth;   %unsharp masking to highligh fine
detail
% figure, imshow(filtered_img(:,:,ceil(size_img(3)/2)),[]) %shows
middle
% slice after sustracting smooth version

%Save in a new directory:
directory_out_img = strcat(directory_image,'_filtered');

if ~isdir(directory_out_img)
    mkdir(directory_out_img);
end


for j = 1 : size_img(3)
    savename= fullfile(directory_out_img,srcFiles(j).name);
    imwrite(uint16(filtered_img(:,:,j)), savename);
end
```

```
%%UNSHARP MASKING CODE

%Ask for image stack directory
directory_image =uigetdir('C:\','Select directory:');

srcFiles = dir(strcat(directory_image,'\*.tif'));  %struct which store
data
%about image stack directory
for i = 1 : length(srcFiles)
    filename = strcat(directory_image,'\',srcFiles(i).name);
    I = imread(filename);
    img(:,:,i) = I; %img is the 3D image
end

size_img=size(img);
```

```
% figure, imshow(img(:,:,ceil(size_img(3)/2)),[]), title('Original
image')
%to show the middle slice of the stack
img = squeeze(img); %it removes singleton dimensions


sigma=2;        %Standard deviation of the Gaussian distribution,
specified
%as a numeric, it refers to FWHM
%size of the filter: 2*ceil(2*sigma)+1 (default)
imgSmooth = imgaussfilt3(img, sigma); %a Gaussian 3D filter is applied

% figure, imshow(imgSmooth(:,:,ceil(size_img(3)/2)),[])  %shows middle
% slice after gaussian
% title('Gaussian filtered image')

filtered_img=2*img-imgSmooth;   %unsharp masking to highligh fine
detail
% figure, imshow(filtered_img(:,:,ceil(size_img(3)/2)),[]) %shows
middle
% slice after sustracting smooth version

%Save in a new directory:
directory_out_img = strcat(directory_image,'_filtered');

if ~isdir(directory_out_img)
    mkdir(directory_out_img);
end


for j = 1 : size_img(3)
    savename= fullfile(directory_out_img,srcFiles(j).name);
    imwrite(uint16(filtered_img(:,:,j)), savename);
end
```

```
%% MASK GENERATOR CODE

function [ mask_2 ] = bkg_mask( I )

I = medfilt2(I, [10 10]);

        % I = medfilt2(I,[M N]) performs median filtering of the matrix
        %     I in two dimensions. Each output pixel contains the
median
        %     value in the 10-by-10 neighborhood around the
corresponding
        %     pixel in the input image. medfilt2 pads the image with
zeros
        %     on the edges, so the median values for the points within
        %     [M N]/2 of the edges may appear distorted.

%h = fspecial('gaussian', [20 20] , 5);
```

```
%I = imfilter(I,h);

n= 2^16;

 [counts,X] = imhist(I,n); %histogram with n bins
% plot(X,counts)
% [COUNTS,X] = imhist(...) returns the histogram counts in COUNTS and
the
%     bin locations in X so that stem(X,COUNTS) shows the histogram.
For
%     indexed images, it returns the histogram counts for each colormap
entry;
%     the length of COUNTS is the same as the length of the colormap.


% mean_val=mean(counts);


[pks,locs] = findpeaks(counts);
[~, pos] = max(pks);
max_peak_loc = locs(pos);

% add 10 % to grayvalues from maximum

margin = 0.10;
bkg_thres = floor(max_peak_loc + (margin*max_peak_loc));


mask = im2bw(I, bkg_thres/2^16);
mask_2 = bwareaopen(mask,100);  %Remove small objects from binary
image: area opening

end
```

```
%%GUIDE FOR ILLUMINATION CORRECTION
function varargout = uno(varargin)
% uno MATLAB code for uno.fig
%      uno, by itself, creates a new uno or raises the existing
%      singleton*.
%
%      H = uno returns the handle to a new uno or the handle to
%      the existing singleton*.
%
%      uno('CALLBACK',hObject,eventData,handles,...) calls the local
%      function named CALLBACK in uno.M with the given input arguments.
%
%      uno('Property','Value',...) creates a new uno or raises the
%      existing singleton*.  Starting from the left, property value
pairs are
%      applied to the GUI before uno_OpeningFcn gets called.  An
%      unrecognized property name or invalid value makes property
application
%      stop.  All inputs are passed to uno_OpeningFcn via varargin.
%
%      *See GUI Options on GUIDE's Tools menu.  Choose "GUI allows only
one
%      instance to run (singleton)".
%
% See also: GUIDE, GUIDATA, GUIHANDLES

% Edit the above text to modify the response to help uno

% Last Modified by GUIDE v2.5 12-Sep-2017 13:53:14

% Begin initialization code - DO NOT EDIT
gui_Singleton = 1;
gui_State = struct('gui_Name',       mfilename, ...
                   'gui_Singleton',  gui_Singleton, ...
                   'gui_OpeningFcn', @uno_OpeningFcn, ...
                   'gui_OutputFcn',  @uno_OutputFcn, ...
                   'gui_LayoutFcn',  [] , ...
                   'gui_Callback',   []);
if nargin && ischar(varargin{1})
    gui_State.gui_Callback = str2func(varargin{1});
end

if nargout
    [varargout{1:nargout}] = gui_mainfcn(gui_State, varargin{:});
else
    gui_mainfcn(gui_State, varargin{:});
end

function uno_OpeningFcn(hObject, eventdata, handles, varargin)
% This function has no output args, see OutputFcn.
% hObject    handle to figure
% eventdata  reserved - to be defined in a future version of MATLAB
% handles    structure with handles and user data (see GUIDATA)
% varargin   command line arguments to uno (see VARARGIN)
```

```
handles.direccion=0;
handles.direccionmask=0;
handles.imageshowed=0;

axes(handles.axes6)
ucm= imread('uc3m.png');
axis off
imshow(ucm,[]);

axes(handles.axes7)
biig= imread('logo.png');
axis off
imshow(biig,[]);



% Choose default command line output for uno
handles.output = hObject;

% Update handles structure
guidata(hObject, handles);

function varargout = uno_OutputFcn(hObject, eventdata, handles)
% varargout  cell array for returning output args (see VARARGOUT);
% hObject    handle to figure
% eventdata  reserved - to be defined in a future version of MATLAB
% handles    structure with handles and user data (see GUIDATA)

% Get default command line output from handles structure
varargout{1} = handles.output;









%%OPEN THE FILE AND MASK DIRECTORIES, AND SHOW THEM IN "?" PUSHBUTTON
function pushbutton_directory_images_Callback(hObject, eventdata,
handles)
% hObject    handle to pushbutton_directory_images (see GCBO)
% eventdata  reserved - to be defined in a future version of MATLAB
% handles    structure with handles and user data (see GUIDATA)
directory_image=handles.direccion;
if directory_image==0;
      directory_image=uigetdir('C:\','Select directory:');
%
directory_image='Z:\Spim_Alicia\Alicia\HEART\TFG\28días\CX14\_dx0.003dz
0.005_ex635_em670_5x_0L_filtered';
      handles.direccion=directory_image;
end
```

```
srcFiles = dir(strcat(directory_image,'\*.tif'));  % struct that store
files data
for i = 1 : length(srcFiles)
    filename = strcat(directory_image,'\',srcFiles(i).name);
    I = imread(filename);
    img(:,:,i) = I; %original image matrix
end
handles.image_orig=img;
handles.img=img;
handles.srcFiles=srcFiles;
handles.direccion=directory_image;
guidata(hObject, handles);

function pushbutton_directory_mask_Callback(hObject, eventdata,
handles)
% hObject    handle to pushbutton_directory_mask (see GCBO)
% eventdata  reserved - to be defined in a future version of MATLAB
% handles    structure with handles and user data (see GUIDATA)
directory_mask=handles.direccionmask;
if directory_mask==0;
    directory_mask=uigetdir('C:\','Select directory:');
%
directory_mask='Z:\Spim_Alicia\Alicia\HEART\TFG\28días\CX14\_dx0.003dz0
.005_ex635_em670_5x_0L_mask(2)';
end
srcFilesmask = dir(strcat(directory_mask,'\*.tif'));  % the folder in
which your images exists

for i = 1 : length(srcFilesmask)
    filename = strcat(directory_mask,'\',srcFilesmask(i).name);
    I = imread(filename);
    I = im2bw(I); %imported mask contains 256 values (although it only
uses 0 as black and 255 as white)
    mask(:,:,i) = I;
end

handles.imageshowed=0;
handles.mask=mask;
handles.srcFilesmask=srcFilesmask;
handles.direccionmask=directory_mask;
guidata(hObject, handles);

function pushbutton_showdirimages_Callback(hObject, eventdata, handles)
% hObject    handle to pushbutton_showdirimages (see GCBO)
% eventdata  reserved - to be defined in a future version of MATLAB
% handles    structure with handles and user data (see GUIDATA)
msgbox(handles.direccion,'Directory of images:');

function pushbutton_showdirmask_Callback(hObject, eventdata, handles)
% hObject    handle to pushbutton_showdirmask (see GCBO)
% eventdata  reserved - to be defined in a future version of MATLAB
% handles    structure with handles and user data (see GUIDATA)
msgbox(handles.direccionmask,'Directory of mask:');
```

```
%%OPEN IMAGE AND MASK STACKS

function slider_stackimages_Callback(hObject, eventdata, handles)
% hObject    handle to slider_stackimages (see GCBO)
% eventdata  reserved - to be defined in a future version of MATLAB
% handles    structure with handles and user data (see GUIDATA)
%                               directory_image =
'srcFiles=handles.srcFiles;\_dx0.001dz0.005_ex635_em670_5x_0L';
%uigetdir('C:\','Select directory:');
%                               srcFiles =
dir(strcat(directory_image,'\*.tif'));  % the folder in which your
images exists
  srcFiles=handles.srcFiles;
  directory_image=handles.direccion;
  img=handles.img;


   axes(handles.axes2);
   axis off;
   set(hObject,'max',length(srcFiles));
   valueslider=ceil(get(hObject,'Value'));
   imageshowed=img(:,:,valueslider);
   imshow(imageshowed);
   set(handles.numberimage, 'String', strcat('Image:
',num2str(valueslider)));
   handles.imageshowed=imageshowed;
   handles.img=img;
   guidata(hObject, handles);

function slider_stackimages_CreateFcn(hObject, eventdata, handles)
% hObject    handle to slider_stackimages (see GCBO)
% eventdata  reserved - to be defined in a future version of MATLAB
% handles    empty - handles not created until after all CreateFcns
called

if isequal(get(hObject,'BackgroundColor'),
get(0,'defaultUicontrolBackgroundColor'))
    set(hObject,'BackgroundColor',[.9 .9 .9]);
end

% --- Executes during object creation, after setting all properties.
function axes5_CreateFcn(hObject, eventdata, handles)
% hObject    handle to axes5 (see GCBO)
% eventdata  reserved - to be defined in a future version of MATLAB
% handles    empty - handles not created until after all CreateFcns
called

% Hint: place code in OpeningFcn to populate axes5
function slider_stackmask_Callback(hObject, eventdata, handles)
% hObject    handle to slider_stackmask (see GCBO)
% eventdata  reserved - to be defined in a future version of MATLAB
% handles    structure with handles and user data (see GUIDATA)
```

```
srcFilesmask=handles.srcFilesmask;
directory_mask=handles.direccionmask;
mask=handles.mask;

axes(handles.axes5);
axis off;
set(hObject,'max',length(srcFilesmask));
valueslider=ceil(get(hObject,'Value'));
maskshowhed=mask(:,:,valueslider);
imshow(maskshowhed);
set(handles.numbermask, 'String', strcat('Mask:
',num2str(valueslider)));
handles.mask=mask;
handles.maskshowhed= maskshowhed;
handles.direccionmask=directory_mask;
guidata(hObject, handles);

function slider_stackmask_CreateFcn(hObject, eventdata, handles)
% hObject    handle to slider_stackmask (see GCBO)
% eventdata  reserved - to be defined in a future version of MATLAB
% handles    empty - handles not created until after all CreateFcns
called

% Hint: slider controls usually have a light gray background.
if isequal(get(hObject,'BackgroundColor'),
get(0,'defaultUicontrolBackgroundColor'))
    set(hObject,'BackgroundColor',[.9 .9 .9]);
end



%%CONTRAST SETTING
function slider_contrast_Callback(hObject, eventdata, handles)
% hObject    handle to slider_contrast (see GCBO)
% eventdata  reserved - to be defined in a future version of MATLAB
% % handles    structure with handles and user data (see GUIDATA)
value=0.002*get(hObject, 'Value');
imageshowed=handles.imageshowed;
img=handles.image_orig;
c=double(imageshowed);
d=value*c;
axes(handles.axes2);
axis off;
imshow(d);
d1=value*double(img);
handles.value=value;
% handles.imageshowed=d;
handles.img=d1;
guidata(hObject, handles);

function slider_contrast_CreateFcn(hObject, eventdata, handles)
% hObject    handle to slider_contrast (see GCBO)
% eventdata  reserved - to be defined in a future version of MATLAB
% handles    empty - handles not created until after all CreateFcns
called
```

```
% Hint: slider controls usually have a light gray background.
if isequal(get(hObject,'BackgroundColor'),
get(0,'defaultUicontrolBackgroundColor'))
    set(hObject,'BackgroundColor',[.9 .9 .9]);
end


%%ROTATION OF IMAGE AND STACK
function pushbutton_rotation_Callback(hObject, eventdata, handles)
% hObject    handle to pushbutton_rotation (see GCBO)
% eventdata  reserved - to be defined in a future version of MATLAB
% handles    structure with handles and user data (see GUIDATA)

    rot=questdlg('Do you want to rotate the stack 90 degrees
clockwise?','Rotation','Rotate', 'Cancel','Cancel');
if rot=='Cancel'
    return;
elseif rot=='Rotate'
    img=handles.img;
    srcFiles=handles.srcFiles;
    directory_image=handles.direccion;
    mask=handles.mask;
    srcFilesmask=handles.srcFilesmask;
    directory_mask=handles.direccionmask;

    stack_size_img = size(img,3);
    stack_size_mask = size(img,3);%should be the same but in any case
        directory_out_img = strcat(directory_image,'_rotated');

        if ~isdir(directory_out_img)
            mkdir(directory_out_img);
        end

        directory_out_mask = strcat(directory_mask,'_rotated');

        if ~isdir(directory_out_mask)
            mkdir(directory_out_mask);
        end
        pathSave_mask = directory_out_mask;

        img_rot = zeros();
    for j = 1 : stack_size_img
        img_rot = rot90(img,3);
        savename= fullfile(directory_out_img,srcFiles(j).name);
        imwrite(uint16(img_rot(:,:,j)), savename);
    end

    mask_rot=zeros();

    for k = 1 : stack_size_mask
        mask_rot = rot90(mask,3);
        savename_mask= fullfile(pathSave_mask,srcFilesmask(k).name);
        imwrite(uint16(mask_rot(:,:,k)), savename_mask);
    end
```

```
    img=img_rot;
    mask=mask_rot;
%
%     axes(handles.axes2);
%     axis off;
%     set(hObject,'max',length(srcFiles));
%     valueslider=ceil(get(hObject,'Value'));
%     imageshowed=img(:,:,valueslider);
%     imshow(imageshowed);
%     set(handles.numberimage, 'String', strcat('Image:
',num2str(valueslider)));
%
%     axes(handles.axes5);
%     axis off;
%     set(hObject,'max',length(srcFilesmask));
%     valueslider=ceil(get(hObject,'Value'));
%     maskshowed=mask(:,:,valueslider);
%     imshow(maskshowed);
%     set(handles.numbermask, 'String', strcat('Mask:
',num2str(valueslider)));
%
    srcFiles = dir(strcat(directory_out_img,'\*.tif'));

    handles.srcFiles=srcFiles;
    handles.img=img;
    handles.direccion=directory_out_img;
    handles.mask=mask;
    handles.direccionmask=pathSave_mask;
    guidata(hObject, handles)
end




%ILLUMINATION CORRECTION
function correction_Callback(hObject, eventdata, handles)
% hObject    handle to correction (see GCBO)
% eventdata  reserved - to be defined in a future version of MATLAB
% handles    structure with handles and user data (see GUIDATA)

%handle imagen
%handle mask
%handle srcfiles
%handle direccion
img=handles.img;
srcFiles=handles.srcFiles;
directory_image=handles.direccion;
mask=handles.mask;



    % Manually
    mu_pixel(1) = transparencia(img(:,:,ceil(end/4)) );
%rounds the elements of X to the nearest integers towards infinity.
```

```
    mu_pixel(2) = transparencia(img(:,:,round(2*end/4)) );
%rounds each element of X to the nearest integer.
    mu_pixel(3) = transparencia(img(:,:,floor(3*end/4)) );
%rounds the elements of X to the nearest integers towards MINUS
infinity.

    mu_mean = mean(mu_pixel);

    % Illumination correccion del stack
    directory_output = strcat(directory_image,'_ill_corrected');
    if ~isdir(directory_output)
        mkdir(directory_output);
    end
    pathSave = directory_output;
    ill_corr = zeros(size(img));
    stack_size = size(img,3);
    for j = 1 : stack_size
        ill_corr(:,:,j)  = illumination_corr(mask(:,:,j), img(:,:,j),
mu_mean);
        savename= fullfile(pathSave,srcFiles(j).name);
        imwrite(uint16(ill_corr(:,:,j)), savename);
    end

function correction_CreateFcn(hObject, eventdata, handles)


% --- Executes during object creation, after setting all properties.
function axes6_CreateFcn(hObject, eventdata, handles)
% hObject    handle to axes6 (see GCBO)
% eventdata  reserved - to be defined in a future version of MATLAB
% handles    empty - handles not created until after all CreateFcns
called
% Hint: place code in OpeningFcn to populate axes6


% --- Executes during object creation, after setting all properties.
function axes7_CreateFcn(hObject, eventdata, handles)
% hObject    handle to axes7 (see GCBO)
% eventdata  reserved - to be defined in a future version of MATLAB
% handles    empty - handles not created until after all CreateFcns
called
```

SOLUTIONS

Recipes of used solutions are presented below.

CUBIC-Reagent 1 (10mL)

Add 3.5 mL of distilled water (35 wt%), 2.5 g of urea (25 wt%) and 2.5 g of N,N,Nâ,Nâtetrakis(2-hydroxy-propyl)ethylenediamine (25 wt%) to a glass beaker. This chemical is highly viscous, so it can be diluted down 1:4 with water. Dissolve the mixture by stirring. This solution does not need to be heated, although increasing the temperature for a short moment will help it to dissolve faster. If it was heated, add 1.5 mL of Triton 100x (15 wt%) when temperature is at room temperature (RT) again and stir. Adjust the weight to 10 g with distilled water to compensate possible water evaporation. Degas the solution with a vacuum pump until air bubbles raised to the surface.

CUBIC-Reagent 2 (10ml)

Add 1.5 mL of distilled water (15 wt%), 1 g of Triethanolamine (10 wt%) and 5 g of Sucrose (50 wt%) to a glass beaker. Let it dissolve on a heated stirrer. Increase the temperature to almost 100ºC. Avoid overheating of the solution. It will dissolve in approximately 30 minutes. When it is almost dissolved, decrease the temperature but keep stirring. Add 2.5 g of urea (25 wt%) and let it dissolve on a non-heated stirrer in order to prevent the decomposition of the urea. Cool down the solution to RT, add 10µL of Triton 100X (0.1%) and stir. Adjust the weight constantly with distilled water. Degas the reagent with a vacuum pump as done for CUBIC-reagent 1. This solution is highly viscous. Thus, submerging the Falcon tube in warm water during the degasification will improve the speed.

PBS in the Concentration 10x (1 L)

- 80.06 g (1.37M) of NaCl
- 1.12 g (15mM) of KCl
- 11.36 g (80 mM) of Na2HPO4
- 3.67 g (27mM) of KH2PO4

Add distilled water up to 1 L. Let it dissolve on a magnetic mixer with a stirring beat.

PBS in the Concentration 1x (1 L)

Add 100 mL of 10X PBS with 900 mL of distilled water. Check the pH and adjust it to pH 7.4 with NaOH (if it is below 7.4) or HCL (if it is above 7.4).

4% PFA Fixative Solution (1 L)

Add 800 mL of PBS 1X to a glass beaker on a stirring plate. Heat up to 55ºC while stirring. Add 40 g of PFA powder to the heated PBS solution. This should be done in a ventilated hood since PFA is toxic. Add a few drops of NaOH with a pipette to support dissolving.

Adjust the volume of the solution to 1 L with PBS 1X. Once the PFA is dissolved, readjust the pH to 7.4 by adding drops of HCl. PFA should be prepared right before the perfusion.

PBT 0.1%Washing Solution (1 L)

Add 1 mL of Triton 100x to 1 L of 1x PBS.

Primary Antibody Solution (20 mL)

Add 0.1 g of Bovine Serum Albumin (BSA) and 0.002 g of Sodium Azida to 20 mL of PBT

0.1%. The solution can be aliquoted in small quantities and stored at -20ºC until used.

Secondary Antibody Solution (20 mL)

Add 0.02 g of Bovine Serum Albumin (BSA) and 0.002 g of Sodium Azide to 20 mL of PBT 0.1%. The solution can be aliquoted in small quantities and stored at -20ºC until used.

AGRADECIMIENTOS

En primer lugar, me gustaría agradecer a Mariví Gómez su constante preocupación, apoyo, motivación y ayuda para que este proyecto saliera adelante. Su presencia en este trabajo no se ha limitado a la tutela del mismo, sino que ha logrado transmitirme la pasión por la investigación y la inquietud de profundizar en los conocimientos adquiridos. Se ha convertido en mi "gurú" de la ciencia y conseguir su tenacidad por el trabajo se ha añadido al conjunto de objetivos que proponía este trabajo.

Por todo lo anterior, agradezco a Manuel Desco por brindarme la oportunidad de entrar en esta pequeña familia que conforma el Laboratorio de Imagen Médica del Hospital Universitario Gregorio Marañón. Su inquietud por aprender y transmitir ha sido un gran referente en este camino.

Gracias a Elisabet y a mis compañeros del LIM y de carrera, no sólo por guiarme y prestarme ayuda siempre que fue necesario, sino por confirmar que el día a día de trabajo durante estos 8 meses nunca fue una obligación sino una elección.

Gracias a mis profesores de la Universidad Carlos III de Madrid por darme todos los conocimientos necesarios para el desarrollo de este trabajo.

Y finalmente, gracias a mis padres por ofrecerme apoyo, cariño y toda clase de facilidades para que pueda cumplir aquello que me propongo, y por ser el origen de mi ambición por aprender. Después de acompañarme en este largo camino habiendo aprendido, reído y sufrido juntos, una parte de ellos es también ahora ingeniera.

Alicia Arévalo García